# Title: Targeting of NAT10 enhances healthspan in a mouse model of human accelerated aging syndrome

Gabriel Balmus[§1,2], Delphine Larrieu[§*1,3], Ana C Barros[1,2], Casey Collins[2], Monica Abrudan[2], Mukerrem Demir[1], Nicola J Geisler[1,2], Christopher J. Lelliott[2], Jacqueline K. White[2], Natasha A Karp[2,4], James Atkinson[5], Andrea Kirton[2], Matt Jacobsen[5], Dean Clift[6], Sanger Mouse Genetics Project[2], Raphael Rodriguez[7,8,9], David J Adams[2], Stephen P Jackson*[1]

§ These authors contributed equally to the work

1. The Wellcome Trust/Cancer Research UK Gurdon Institute and Department of Biochemistry, University of Cambridge, CB2 1QN, United Kingdom.

2. The Wellcome Trust Sanger Institute, Hinxton, Cambridge, CB10 1SA, United Kingdom.

3. Current address: Cambridge Institute for Medical Research, Department of clinical biochemistry, University of Cambridge, CB2 0XY, United Kingdom.

4. Discovery Sciences, IMED Biotech Unit, AstraZeneca, Cambridge, UK

5. Drug Safety and Metabolism, IMED Biotech Unit, AstraZeneca, Cambridge UK

6. Laboratory of Molecular Biology, Cambridge, CB2 OQH, United Kingdom.

7. Institut Curie, PSL Research University, Paris Cedex 05, France.

8. CNRS UMR3666, 75005 Paris, France.

9. INSERM U1143, 75005 Paris, France.

* Correspondence to s.jackson@gurdon.cam.ac.uk and dl437@cam.ac.uk

**Abstract**

Hutchinson-Gilford Progeria Syndrome (HGPS) is a rare but devastating genetic disease characterized by segmental premature aging, with cardiovascular disease being the main cause of death. Cells from HGPS patients accumulate progerin, a permanently farnesylated, toxic form of Lamin A, disrupting nuclear shape and chromatin organization, leading to DNA-damage accumulation and senescence. Therapeutic approaches targeting farnesylation or aiming to reduce progerin levels have provided only partial health improvements. Recently, we identified Remodelin, a small-molecule agent that leads to amelioration of HGPS cellular defects through inhibition of the enzyme N-acetyltransferase 10 (NAT10). Here, we show preclinical data demonstrating that targeting NAT10 in vivo, either via chemical inhibition or genetic depletion, significantly enhances cardiac function, fitness and healthspan in a *Lmna*$^{G609G}$ HGPS mouse model. Collectively, the data provided here highlight NAT10 as a potential therapeutic target for HGPS.

## Introduction

The nuclear envelope (NE) provides a dynamic boundary between the inner nuclear mass and the cytoplasm, and is critical for normal functioning of the eukaryotic cell. Key factors for NE function as a compartmental border are the nuclear lamins, scaffold proteins that specify nuclear architecture and provide mechanical strength to the nucleus and cell [1]. Notably, over the past few years, lamins have emerged as significant players in many other critical cellular functions including differentiation, intracellular signaling, chromatin organization, transcription, as well as DNA replication and repair [2,3]. In mammals, the nuclear lamins are categorized in two distinct classes: A-type lamins (Lamin A, Lamin C, Lamin C2 and Lamin AΔ10 all encoded by the *LMNA* gene) and B-type lamins (Lamin B1 encoded by *LMNB1*, and Lamin B2 that, together with Lamin B3, are encoded by the *LMNB2* gene) [4].

In accord with their important roles, loss-of-function mutations in lamin genes result in genetic syndromes with severe presentations called laminopathies (OMIM #150330; #150340; #150341). These include muscular dystrophies (for example, Emery-Dreyfus Muscular Dystrophy), peripheral neuropathies (for example, Charcot-Marie Tooth-Disease), leukodystrophy, lipodystrophy, as well as premature aging (progeria) syndromes such as Atypical Werner Syndrome (AWS), Restrictive Dermopathy (RD) and Hutchinson Gilford Progeria Syndrome (HGPS) [2,5]. Of all these syndromes, HGPS is the one with the most striking presentation.

After onset, usually within the first year of life, HGPS patients start to display short stature, low body weight, hair loss, lipodystrophy, scleroderma, decreased mobility, osteoporosis, as well as facial features that resemble accelerated aspects of normal ageing [6]. While cognitive development is normal, cardiovascular abnormalities – characterized by medial smooth-muscle cell loss and secondary maladaptive vascular

remodeling (intimal thickening, disrupted elastin fibers and deposition of atherosclerotic plaques) – are the main reasons for death, with the median life expectancy at birth for HGPS patients being 14.6 years [7-10].

HGPS arises from heterozygous G608G point mutation of *LMNA* exon 11*,* leading to cryptic mRNA splicing and expression of a shorter, dysfunctional form of Lamin A called progerin [11-13]. Like wild-type Lamin A, progerin undergoes several post-translational modifications, including the addition of a farnesyl group required for its targeting to the nuclear envelope. However, unlike Lamin A, progerin remains permanently farnesylated, causing it to accumulate at the inner nuclear membrane. In HGPS cells, progerin acts as a dominant-negative protein, aggregating wild-type lamins, disrupting nuclear shape and chromatin organization, and leading to increased genomic instability and rapid cell senescence [14,15]. While farnesyl-transferase inhibition (FTI) [16-20] is being explored as a therapeutic approach for HGPS and has provided certain health improvements in patients [21], there is a clear need for additional therapeutic regimes [22]. Recently, we discovered that a small-molecule compound, which we named Remodelin, can ameliorate HGPS cellular phenotypes. Remodelin acts in a progerin- and FTI-independent pathway by targeting and inhibiting the N-acetyltransferase NAT10 [23].

Here, we assess NAT10 inhibition as a potential therapeutic strategy for HGPS by using an established mouse model (*Lmna - G609G* allele) that exhibits premature-aging phenotypes similar to those of HGPS patients [24]. Critical for translating NAT10 inhibition towards human patients, we show that chemical or genetic targeting of NAT10 decreases genomic instability*,* and improves global healthspan of both homozygous and heterozygous HGPS mice.

## Results

### Remodelin is well tolerated and extends HGPS mouse health

To determine the effects of Remodelin on HGPS mouse cells, we derived skin fibroblasts from *Lmna*$^{G609G/G609G}$ and wild-type (WT) littermates. As observed in human HGPS fibroblasts [25,26], *Lmna*$^{G609G/G609G}$ fibroblasts displayed nuclear shape defects and increased genomic instability as reflected by a higher level of the DNA double-strand break (DSB) marker γH2AX (Ser-139 phosphorylated histone H2AX), in a manner that was abrogated by Remodelin treatment (Fig. 1a, b). These results showed that Remodelin treatment can reverse HGPS induced genomic instability and nuclear shape defects in mouse cells, and provided us with encouraging preliminary evidence to proceed with *in vivo* studies. To assess Remodelin's suitability for *in vivo* studies, we initially defined its pharmacokinetic properties in WT mice. Overall, oral (PO) delivery appeared the best route of administration (Fig. 1c; Supplementary Fig. 1a*;* Supplementary Table 1-2), with bioavailability of ~44% (Fig. 1c, d) and significant accumulation to heart and skeletal muscle (Fig. 1e). Based on these data, WT and *Lmna*$^{G609G/G609G}$ mice were treated with a Remodelin dose of 100 mg per kg orally, on a daily schedule from 3 weeks of age onwards, until endpoint. This treatment was well tolerated by both genotypes, with no weight loss (Supplementary Fig. 1b) and with significant Remodelin being present in the skeletal muscle, liver and brain of the *Lmna*$^{G609G/G609G}$ mice (Supplementary Fig. 1c). Furthermore, in line with a previous report that NAT10 promotes melanogenesis [27], we found that Remodelin treatment led to hair graying (Supplementary Fig. 1d). As described before, we found that *Lmna*$^{G609G/G609G}$ mice had dramatically shorter healthspans compared to WT controls, associated with accelerated body-weight loss (Fig. 1f*;* Supplementary Table 3) and premature-aging phenotypes resembling the human syndrome [24]. Notably, Remodelin

led to a 25% increase in Kaplan–Meier area under the curve for treated versus vehicle treated mice (Fig. 1f; Supplementary Table 3). Together, these data established that Remodelin is well tolerated *in vivo* and can enhance the healthspan of HGPS mice.

**Remodelin ameliorates cardiac pathology of HGPS mice**

HGPS clinical presentation involves loss of subcutaneous adipose tissue[7] and cardiovascular abnormalities, including adventitial fibrosis and medial smooth-muscle cell loss with depletion of smooth-muscle actin in the remaining cells [8,9,28,29]. These cardiovascular features represent major pathologies that contribute to morbidity and lethality in HGPS[2]. Thus, we analyzed these parameters at the level of the skin, aorta and coronary heart arteries in Remodelin-treated HGPS mice as compared to vehicle treated controls at their respective end-points. Importantly, Remodelin treatment significantly reduced the loss of subcutaneous adipose tissue that is seen in the HGPS mouse model (Fig. 2a). Moreover, it led to dramatic amelioration of HGPS cardiac pathologies, including reduction of adventitial fibrosis of the aorta (Fig. 2b), rescue of vascular smooth muscle cell loss (Fig. 2c) and salvage of smooth muscle actin (SMA) loss both in the aorta and coronary arteries (Fig. 2d*,* Supplementary Fig. 2a). By contrast, Remodelin treatment had no significant effect on WT mice at a similar age (Supplementary Fig. 2b). Furthermore, as observed in mouse and human fibroblasts, Remodelin reduced markers of genome instability in both heart and lung tissues of *Lmna*$^{G609G/G609G}$ mice (Fig. 2e, f). Together, these data highlighted how Remodelin treatment delayed onset of cardiovascular pathologies that represent the most debilitating aspect of HGPS.

**Engineering and characterization of a *Nat10* mouse model**

To validate NAT10 was the relevant pharmacological target mediating the *in vivo* effects of Remodelin, we engineered a *Nat10* knockout mouse model (Supplementary Fig. 3a). Bi-allelic *Nat10* inactivation was lethal before embryonic day E14.5 (Fig. 3a), indicating that NAT10 is critical for mouse development. However, heterozygous *Nat10*$^{+/-}$ mice were born healthy, and were observed to express the *Nat10* mRNA and protein products at levels ~50% of those in WT animals (Fig. 3b, c). As NAT10 is largely uncharacterized and has not been studied in mice before, we performed a broad phenotypic analysis of *Nat10*$^{+/-}$ mice (Supplementary Fig. 3b, c, Supplementary Fig. 4 and, Supplementary Data file 1). In most regards, *Nat10*$^{+/-}$ mice were indistinguishable from WT (blue color Supplementary Fig. 3b), with the exception of body weight, which was consistently lower than that of WT mice despite similar tail-to-nose lengths, associated with changes in lean and fat mass, triglycerides and cholesterol levels (Supplementary Fig. 3b, Supplementary Fig. 4a). Additional parameters, including potassium levels and neutrophil numbers, showed evidence of sexual dimorphism (Supplementary Fig. 4b). Moreover, NAT10 reduction triggered gene-expression changes in the heart (Fig. 3d, Supplementary Data file 2), with many deregulated genes being connected to cellular pathways associated with longevity, such as responses to starvation or insulin signaling[30] (Supplementary Fig. 3c). Other highly enriched pathways deregulated upon NAT10 depletion included regulation of inclusion body assembly and protein refolding. These data showed that, while complete NAT10 knock-out leads to embryonic lethality, NAT10 haploinsufficient mice are born at expected frequencies and are overtly healthy, thereby allowing us to explore potential impacts of reducing *Nat10* gene dosage in the context of a HGPS *in vivo* genetic model.

### *Nat10* haploinsufficiency enhances fitness of progeria mice

To explore the interaction between NAT10 and HGPS, we generated two cohorts of *Lmna*$^{G609G/G609G}$ mice: one on a WT *Nat10* background (*Nat10*$^{+/+}$) and the other carrying the *Nat10* heterozygous deletion (*Nat10*$^{+/-}$). Notably, healthspan analysis showed that, as for Remodelin treatment, reduced *Nat10* gene dosage significantly extended the timeframe of body weight loss of *Lmna*$^{G609G/G609G}$ by 17% (Fig. 4a; Supplementary Table 3). Moreover, as compared to *Lmna*$^{G609G/G609G}$ animals, *Lmna*$^{G609G/G609G}$*Nat10*$^{+/-}$ mice displayed a significant delay in the appearance of back curvature (Fig. 4b-d) and enhanced fitness, as observed by lower incidence of common *Lmna*$^{G609G/G609G}$ mouse pathologies such as penile prolapse and eye keratitis (data not shown). Additionally, *Lmna*$^{G609G/G609G}$*Nat10*$^{+/-}$ mice were more active and overtly healthier than their age-matched controls (Supplementary Movies 1-3). To better understand how HGPS phenotypes were counteracted by NAT10 depletion, we performed selected biochemical analyses on mice at 9 and 12 weeks of age. While NAT10 depletion had no effects on parameters such as fat mass and cholesterol levels of progeria mice, it significantly normalized others, including glycerol and urea levels (Supplementary Data file 3). Furthermore, the decrease in heart rate observed in *Lmna*$^{G609G/G609G}$ mice compared to WT controls was significantly circumvented by *Nat10* depletion at 9 weeks but not at 12 weeks (Fig. 4e), suggesting that the onset of heart abnormalities was delayed. Notably, at 12 weeks, *p21* expression was increased in hearts of *Lmna*$^{G609G/G609G}$ mice as compared to WT controls, probably reflecting higher DNA-damage loads, but not in *Lmna*$^{G609G/G609G}$*Nat10*$^{+/-}$ mice (Fig. 4f). While *Lmna*$^{G609G/G609G}$ mice were reported to be infertile [24], under our husbandry they were sub-fertile: *Lmna*$^{G609G/G609G}$ males had decreased sperm counts (Supplementary Fig.

5a) but sperm were motile and able to fertilize wild-type oocytes (Supplementary Fig. 5b). Similarly, *Lmna*$^{G609G/G609G}$ females produced morphologically normal oocytes that were meiotically competent (Supplementary Fig. 5c, d), and super-ovulated eggs from *Lmna*$^{G609G/G609G}$ females could be fertilized by WT sperm (Supplementary Fig. 5b). However, while *Lmna*$^{G609G/G609G}$ females never produced litters, *Lmna*$^{G609G/G609G}$ males could father pups, albeit at a very low frequency and never more than one litter. These data suggested that sub-fertility of HGPS mice was caused by decreased reproductive fitness rather than by a specific physiological problem. Strikingly, global fitness/health improvements associated with reduced *Nat10* gene dosage in *Lmna*$^{G609G/G609G}$*Nat10*$^{+/-}$ mice (Supplementary Movies 2-3) correlated with an enhancement of male and female fertility (Supplementary Fig. 5e; 45% in *Lmna*$^{G609G/G609G}$*Nat10*$^{+/-}$ versus 21% in *Lmna*$^{G609G/G609G}$). While we, like others, have used homozygous *Lmna*$^{G609G/G609G}$ to model HGPS, it is important to note that patients carry a heterozygous *Lmna* mutation, leading to expression of both WT Lamin A and progerin. We therefore wished to study the effect of reducing *Nat10* gene dosage in heterozygous *Lmna*$^{+/G609G}$ mice. Extending upon the previous report showing reduced lifespan of such mice[24], we performed an extensive phenotypic analysis of *Lmna*$^{+/G609G}$ mice and found them to display similar premature aging phenotypes as the homozygous mutant (Supplementary Fig. 6, Supplementary Data file 4), albeit with delayed onset. When we assessed the impact of *Nat10* heterozygosity in this human-disease model, we found that *Lmna*$^{+/G609G}$*Nat10*$^{+/-}$ mice had significantly longer healthspan than *Lmna*$^{+/G609G}$*Nat10*$^{+/+}$ mice. Indeed, there was a 90 days gap between the longest lived *Lmna*$^{G609G/+}$*Nat10*$^{+/-}$ mouse and the longest lived *Lmna*$^{+/G609G}$*Nat10*$^{+/+}$ mouse (Fig. 4g*;* Supplementary Table 3). In addition, the *Lmna*$^{G609G/+}$*Nat10*$^{+/-}$ mice displayed health enhancements, such as decreased back curvature (Supplementary Fig. 7).

**Identification of readouts for NAT10 inhibition in HGPS**

To investigate the impacts of NAT10 inhibition *in vivo*, and as the main cause of death in HGPS patients is due to heart dysfunction, we performed global gene-expression analyses on tissues derived from hearts of *Lmna*$^{G609G/G609G}$*Nat10*$^{+/-}$ and Remodelin treated *Lmna*$^{G609G/G609G}$ mice compared to their respective controls (Supplementary Data file 5). This work identified a specific set of genes (Supplementary Fig. 8a) – largely connected to metabolic pathways (Supplementary Fig. 8b) – as significantly up-regulated (blue) or down-regulated (red) in *Lmna*$^{G609G/G609G}$ mice compared to WT (Supplementary Fig. 8a, lane 1). Interestingly, some of these gene-expression differences (* in Supplementary Fig. 8a) were counteracted by both Remodelin treatment (row 2) and *Nat10* depletion (row 3), suggesting that these might comprise a gene-expression signature for amelioration of HGPS pathologies by NAT10 inhibition. Collectively, these data highlighted a strong correlation between NAT10 chemical inhibition or its genetic depletion on cellular imbalances caused by the *Lmna*$^{G609G/G609G}$ HGPS mutation. They also suggested the potential for gene-expression signatures as biomarkers for HGPS and its alleviation.

As acetylation of α-tubulin lysine 40 (K40) is a documented NAT10 target[31,32], we evaluated it as a potential readout for NAT0 inhibition *in vivo*. Indeed, quantitative analyses established that patient-derived HGPS fibroblasts, as well as *Lmna*$^{G609G/G609G}$ mouse-derived skin cells and tissues, displayed increased acetyl-α-tubulin K40 when compared to WT controls (Fig. 5; Supplementary Fig. 9), probably associated with increased microtubule stability contributing to HGPS cellular phenotypes[25]. However, this was not associated with a significant and consistent increased NAT10 protein levels, suggesting that NAT10 enzymatic activity might be elevated, leading to

increased α-tubulin acetylation. In line with these findings, Remodelin treatment or reduced *Nat10* gene dosage decreased acetyl-α-tubulin K40 levels in extracts from cells and mouse tissues (Fig. 5a, b; Supplementary Fig. 9a), in cultured cells (Fig. 5c), and as detected by *in situ* mouse-tissue staining (Fig. 5d; Supplementary Fig. 9b-d). These results thus indicated that α-tubulin K40 acetylation is increased in both human HGPS cells and in the mouse HGPS model in a manner counteracted by Remodelin treatment, thereby suggesting this acetylation mark as a potential disease biomarker and a readout for NAT10 inhibition *in vivo*.

## Discussion

HGPS, a debilitating premature aging disease whose features strikingly resemble accelerated aspects of normal aging, represents a paradigm for translational medicine in the arena of aging research [33]. The complex nature of this segmental syndrome makes it difficult to target therapeutically, with standard therapeutic approaches mainly aiming at preventing the expression or the accumulation of progerin at the nuclear envelope. Thus, strategies that have so far received most attention largely involve targeting enzymes participating in the progerin pathway [10], including HMG-CoA reductase, farnesyl-pyrophosphate synthase, farnesyl transferase [21], isoprenylcysteine carboxyl methyltransferase, as well as modulating *Lmna* pre-mRNA splicing by morpholino compounds [24]. Notably, there is encouraging evidence that HGPS children treated with the FTI lonafarnib display improved vascular stiffness and bone structure [21], as well as 33% increased survival based on Kaplan–Meier area under the curve estimations [10]. Because FTI treatment is now essentially standard-of-care and the HGPS patient population is small (~1 in 18 million) [34], further clinical trials will likely be arranged as combined therapies with lonafarnib [22].

The results we have presented here show that NAT10 genetic depletion or its chemical inhibition by the compound Remodelin leads to healthspan and fitness improvements in both homozygous and heterozygous HGPS mice *via* a mechanism that appears to be independent of progerin. Reinforcing our conclusions, we have recently carried out further studies with a Remodelin derivative, Remodelin-fluor (Supplementary Fig. 10a), that in HGPS cells showed the same effect as Remodelin at half the Remodelin dose (Supplementary Fig. 10b). Using this compound in mice, we observed hair graying (Supplementary Fig. 10c) and no drug-induced weight loss (Supplementary Fig. 10d). Moreover, Remodelin-fluor treatment led to a significant decrease in the timeframe of

body weight loss with 30% increase in Kaplan–Meier area under the curve for treated mice as compared to vehicle treated mice (Supplementary Fig. 10e*;* Supplementary Table 3).

While we did not see Remodelin-induced effects on low mineral density and bone mineral content in HGPS mice (see Supplementary Data file 3), we observed significant disease amelioration by Remodelin treatment and *Nat10* genetic depletion in critical organs such as the heart. Notably, these cardiovascular effects were not only restricted to the aorta but also included impacts on other large vessels of the heart, such as the coronary arteries. These effects are of potential clinical relevance because advanced coronary disease is prevalent in HGPS patients, even in the absence of high blood pressure [29,35]. We also note that, in contrast to FTI[36], Remodelin decreases markers of genome instability in HGPS cells and organs. We showed in our previous work that combining FTI and Remodelin in HGPS patient cells does not improve the cellular phenotypes further compared to Remodelin alone (see Supplementary Fig. 8 of Larrieu et al., Science 2014 – reference 25). However, as they act in different pathways, it is possible that the phenotypes *in vivo* would benefit from the drug combination, which will likely be the scope of ensuing studies. Collectively, our data thus highlight the potential for NAT10 inhibitors in treating HGPS in combination with lonafarnib, where additive therapeutic effects might be anticipated.

While we found that complete *Nat10* deletion resulted in early embryonic lethality in mice, *Nat10* haploinsufficiency or chemical inhibition *via* Remodelin treatment did not confer any profound side effects. Because NAT10 is a 115 kDa protein with multiple functional domains, it could be that the lethality associated with its total loss is linked to an aspect of the NAT10 protein other than its N-acetyltransferase function. In this regard, we note that in *Caenorhabditis elegans*, a null allele of NAT10, *nath-*

*10*(*tm2624*), causes fully penetrant embryonic lethality in the homozygous state. By contrast, the *nath-10*(*N2*) hypomorphic allele containing a polymorphism in the N-acetyltransferase domain did not cause pathology in a homozygous setting, but instead conferred increased fitness and a strong competitive advantage over WT animals[37]. While these and our data are encouraging from the perspective of considering NAT10 inhibition as a therapeutic approach for HGPS, the fact that our understanding of NAT10 biology is still in its infancy means that any clinical studies should be explored with caution.

The small number of HGPS patients and the diverse nature of their pathologies provide challenges for the evaluation of potential new HGPS therapies in the clinic [22]. If and when NAT10 inhibitors are explored in clinical settings, it will thus be extremely valuable to be able to assess target engagement. In this regard, we have identified gene-expression signatures that are associated with HGPS cells and which are rebalanced towards WT by either Remodelin treatment or NAT10 depletion. Furthermore, we have highlighted the potential for acetylated α-tubulin lysine 40 (K40), a known NAT10 target [31,32], as a biomarker for NAT10 inhibition in cells and *in vivo*. These findings also correlated with our previous data indicating that NAT10 inhibition ameliorates HGPS cellular phenotypes, at least in part by mediating microtubule destabilization [25]. Since α-tubulin acetylation at K40 is elevated in HGPS tissues and cells compared to controls, it will be of interest to explore whether this biomarker could be used to monitor disease progression and also enhance our understanding of disease patho-biology. Finally, we note that because the hallmarks of HGPS are present at lower levels in the vasculature and other tissues of aged normal individuals[33], NAT10 targeting might offer therapeutic opportunities in broader settings. In accord with such a possibility, we have recently reported effects of NAT10 inhibition

in normally aged smooth muscle cells [26], that support the potential for NAT10 inhibition in the context of normal ageing.

## Methods

### Synthesis of Remodelin and derivatives

All solvents and reagents were purified by using standard techniques or used as supplied from commercial sources (Sigma-Aldrich). NMR spectra were acquired on a Bruker 500 MHz instrument with deuterated solvents at 300 K. Notation for the $^{1}$H NMR spectral splitting patterns includes: singlet (s), doublet (d), triplet (t), broad (br) and multiplet/overlapping peaks (m). Signals are quoted as values in ppm and coupling constants (J) are quoted in Hertz. Mass spectra were recorded on a Micromass® Q-Tof (ESI) spectrometer. The general procedure is highlighted in the Supplemental Material and Methods section.

### Animals

The care and use of all mice used to generate data for this protocol was carried out in accordance with UK Home Office regulations, UK Animals (Scientific Procedures) Act of 2013 under UK Home Office licenses which approved this which were reviewed regularly by the WTSI Animal Welfare and Ethical Review Board. Mice carrying the knockout-first conditional-ready allele *Nat10*$^{tm1a(KOMP)Wtsi}$ (abbreviated to *Nat10*$^{tm1a}$) were generated on a C57BL/6N background as part of the Sanger Mouse Genetics Project (MGP). *Lmna*$^{G609G}$ (C57BL/6N) mice were imported from the laboratory of Carlos-Lopez Otin [24] and re-derived on the line C57BL/6NTac at the Wellcome Trust Sanger Institute (WTSI). Mice were euthanized by $CO_2$ inhalation followed by cervical dislocation. Mouse experimental procedures including oocyte culture and immunofluorescence, generation of oocytes and *in-vitro* fertilization, heart rate comparison, kyphosis index calculation, immunoblotting, immunofluorescence and

immunohistochemistry along other details on animal experimental methods are highlighted in the Supplemental Material and Methods section.

**Assessment of Remodelin toxicity *in vivo* and dosing**

Remodelin toxicity was assessed by Crown Biosciences on twelve 6 weeks old C57BL/6N female mice, with a body weight of 20g on average (animal supplier: Shanghai Laboratory Animal Center (SLAC, Shanghai, China): see Table S2. At WTSI, Remodelin and Remodelin Fluor were dissolved in a solution of 20% DMSO, 65% (45% 2-Hydroxypropyl-b-cyclodextrin solution, H5784 Sigma Aldrich) and 15% Tween 80 (P8074 Sigma Aldrich). The "vehicle" treated animals were given this solution alone, without Remodelin. Remodelin and Remodelin Fluor were administered daily by oral gavage at 100mg per kg per day and 50mg per kg per day respectively (defined as non-toxic doses in toxicity studies), from day 21 and until culled. Additional details on animal experimental methods are highlighted in the Supplemental Material and Methods section.

**Cell lines**

Normal skin primary fibroblasts GM03440 and Hutchinson Gilford Progeria Syndrome (HGPS) skin primary fibroblasts AG11513 were purchased from Coriell Cell Repositories and used between passage number 9-17. Cells were grown in Dulbecco's modified Eagle medium (DMEM, Sigma-Aldrich) supplemented with 10% fetal bovine serum (BioSera), 2mM L-glutamine, 100U per ml penicillin, 100 µg $ml^{-1}$ streptomycin. All cell lines have been tested for mycoplasma contamination using Charles River Mycoplasma Testing Services.

**RNA extraction, qPCR analysis and RNAseq**

RNA was extracted from tissues from n>5 independent mice per group using the RNeasy fibrous tissue mini kit (50) (cat. No.7404; Qiagen) and quantified using the NanoDrop 1000 Spectrophotometer (Thermo Fisher Scientific). 2µg RNA per sample was used to produce cDNA using the High-Capacity RNA-to-cDNA kit (cat. No. 4387406; Applied Biosystems/Thermo Fisher Scientific). qPCR was carried out using the TaqMan system (Universal Master Mix II, with UNG, 4440038; Applied Biosystems/Thermo Fisher Scientific) on an Applied Biosystems Quant Studio 3 machine. n≥3 mice were used for each genotype, with 50ng cDNA for each sample run in triplicate or quadruplicate. For RNAseq transcriptome data was obtained using paired end sequencing, with read lengths of 150 bp, on a NextSeq 500 machine. Trimmed reads were aligned using STAR aligner (version 2.4.2a) to the mouse genome assembly GRCm38. Additional details on RNA qPCR and RNAseq methods are highlighted in the Supplemental Material and Methods section.

**Antibodies**

Antibodies used in this study are: Lamin A/C (sc-6215 Santa-Cruz 1:200 for Western Blotting and 1:100 for Immunofluorescence), NAT10 (13365-1-AP ProteinTech Europe 1:400 for Western Blotting), γH2AX (05-636 Millipore, 1:200 for Western Blotting and 1:100 for Immunofluorescence), H2AX (ab11175 Abcam, 1:500 for Western Blotting), β Actin (ab8226, Abcam, 1:1000 for Western Blotting), Acetyl α Tubulin (K40) (5335 Cell Signalling, 1:500 for Western Blotting and 1:100 for Immunofluorescence), α Tubulin (T9026 Sigma-Aldrich, 1:1000 for Western Blotting and 1:400 for Immunofluorescence), Nup98 (Abcam, ab50610 1:100 for Immunofluorescence) and tyrosinated-α-tubulin (YOL1/34, AbD Serotec, 1:200 for Immunofluorescence).

**Statistical analysis**

For all analyses, the individual mouse was considered the experimental unit within the studies. Survival distributions of the different cohorts was plotted using the Kaplan–Meier estimator and statistical analysis was performed using log-rank (Mantel-Cox) test. For survival analysis, we have completed power calculations for a large size effect and with an n of 10 per group. We could detect a 0% to 60% change in survival after treatment, 91% of the time (power of Fisher Exact test, 0.91). To meet the assumption of this statistical method, censoring of an individual mouse could only occur when the culling of a mouse was not related to the genotype/assessed-phenotype (e.g. fight wound leading to overt clinical presentation). Additional details on the high throughput phenotyping screens are highlighted in the Supplemental Material and Methods section.

**Data availability**

The mouse phenotypic data from the present manuscript are available in the supplementary Data files. Mouse phenotypic data will be available from IMPC (http://www.mousephenotype.org/). RNAseq data will be available from GEO public repository (https://www.ncbi.nlm.nih.gov/geo/).

**Supplementary Material**

Additional Material and Methods; Supplementary Figures 1 to 10; Supplementary Tables 1 to 4; Supplementary Data files 1 to 5; Supplementary Movies 1 to 3

**References**


1. Osmanagic-Myers, S., Dechat, T. & Foisner, R. Lamins at the crossroads of mechanosignaling. *Genes & Development* **29,** 225–237 (2015).
2. Gonzalo, S., Kreienkamp, R. & Askjaer, P. Hutchinson-Gilford Progeria Syndrome: A premature aging disease caused by LMNA gene mutations. *Ageing Res. Rev.* **33,** 18–29 (2017).
3. Ungricht, R. & Kutay, U. Mechanisms and functions of nuclear envelope remodelling. *Nat. Rev. Mol. Cell Biol.* **18,** 229–245 (2017).
4. Burke, B. & Stewart, C. L. The nuclear lamins: flexibility in function. *Nat. Rev. Mol. Cell Biol.* **14,** 13–24 (2013).
5. Capell, B. C. & Collins, F. S. Human laminopathies: nuclei gone genetically awry. *Nature Reviews Genetics* **7,** 940–952 (2006).
6. Hennekam, R. C. M. Hutchinson-Gilford progeria syndrome: review of the phenotype. *Am. J. Med. Genet. A* **140,** 2603–2624 (2006).
7. Merideth, M. A. *et al.* Phenotype and course of Hutchinson-Gilford progeria syndrome. *N. Engl. J. Med.* **358,** 592–604 (2008).
8. Stehbens, W. E., Wakefield, S. J., Gilbert-Barness, E., Olson, R. E. & Ackerman, J. Histological and Ultrastructural Features of Atherosclerosis in Progeria. *Cardiovascular Pathology* **8,** 29–39 (1999).
9. Stehbens, W. E., Delahunt, B., Shozawa, T. & Gilbert-Barness, E. Smooth muscle cell depletion and collagen types in progeric arteries. *Cardiovascular Pathology* **10,** 133–136 (2001).
10. Gordon, L. B. *et al.* Impact of farnesylation inhibitors on survival in Hutchinson-Gilford progeria syndrome. *Circulation* **130,** 27–34 (2014).
11. Eriksson, M. *et al.* Recurrent de novo point mutations in lamin A cause

Hutchinson-Gilford progeria syndrome. *Nature* **423,** 293–298 (2003).

12. Paola Scaffidi, T. M. Reversal of the cellular phenotype in the premature aging disease Hutchinson-Gilford Progeria Syndrome. *Nat. Med.* **11,** 440–445 (2005).
13. De Sandre-Giovannoli, A. *et al.* Lamin a truncation in Hutchinson-Gilford progeria. *Science* **300,** 2055–2055 (2003).
14. López-Otín, C., Blasco, M. A., Partridge, L., Serrano, M. & Kroemer, G. The Hallmarks of Aging. *Cell* **153,** 1194–1217 (2013).
15. Cohen, T. V., Hernandez, L. & Stewart, C. L. Functions of the nuclear envelope and lamina in development and disease. *Biochem. Soc. Trans.* **36,** 1329–1334 (2008).
16. Glynn, M. W. & Glover, T. W. Incomplete processing of mutant lamin A in Hutchinson–Gilford progeria leads to nuclear abnormalities, which are reversed by farnesyltransferase inhibition. *Hum. Mol. Genet.* **14,** 2959–2969 (2005).
17. Yang, S. H. *et al.* Blocking protein farnesyltransferase improves nuclear blebbing in mouse fibroblasts with a targeted Hutchinson–Gilford progeria syndrome mutation. *PNAS* **102,** 10291–10296 (2005).
18. Toth, J. I. *et al.* Blocking protein farnesyltransferase improves nuclear shape in fibroblasts from humans with progeroid syndromes. *PNAS* **102,** 12873–12878 (2005).
19. Capell, B. C. *et al.* Inhibiting farnesylation of progerin prevents the characteristic nuclear blebbing of Hutchinson-Gilford progeria syndrome. *PNAS* **102,** 12879–12884 (2005).
20. Blondel, S. *et al.* Drug screening on Hutchinson Gilford progeria pluripotent stem cells reveals aminopyrimidines as new modulators of farnesylation. *Cell Death & Disease* **7,** e2105 (2016).

21. Gordon, L. B. *et al.* Clinical trial of a farnesyltransferase inhibitor in children with Hutchinson-Gilford progeria syndrome. *Proc. Natl. Acad. Sci. U.S.A.* **109,** 16666–16671 (2012).

22. Gordon, L. B., Kieran, M. W., Kleinman, M. E. & Misteli, T. The decision-making process and criteria in selecting candidate drugs for progeria clinical trials. *EMBO Mol Med* **8,** 685–687 (2016).

23. Larrieu, D., Britton, S., Demir, M., Rodriguez, R. & Jackson, S. P. Chemical inhibition of NAT10 corrects defects of laminopathic cells. *Science* **344,** 527–532 (2014).

24. Osorio, F. G. *et al.* Splicing-directed therapy in a new mouse model of human accelerated aging. *Sci Transl Med* **3,** 106ra107–106ra107 (2011).

25. Larrieu, D., Britton, S., Demir, M., Rodriguez, R. & Jackson, S. P. Chemical inhibition of NAT10 corrects defects of laminopathic cells. *Science* **344,** 527–532 (2014).

26. Cobb, A. M. *et al.* Prelamin A impairs 53BP1 nuclear entry by mislocalizing NUP153 and disrupting the Ran gradient. *Aging Cell* **15,** 1039–1050 (2016).

27. Oh, T.-I., Lee, Y.-M., Lim, B.-O. & Lim, J.-H. Inhibition of NAT10 Suppresses Melanogenesis and Melanoma Growth by Attenuating Microphthalmia-Associated Transcription Factor (MITF) Expression. *Int J Mol Sci* **18,** 1924 (2017).

28. Varga, R. *et al.* Progressive vascular smooth muscle cell defects in a mouse model of Hutchinson-Gilford progeria syndrome. *PNAS* **103,** 3250–3255 (2006).

29. Olive, M. *et al.* Cardiovascular pathology in Hutchinson-Gilford progeria: correlation with the vascular pathology of aging. *Arterioscler. Thromb. Vasc. Biol.* **30,** 2301–2309 (2010).

30. Vermeij, W. P. *et al.* Restricted diet delays accelerated ageing and genomic stress in DNA-repair-deficient mice. *Nature* **537,** 427–431 (2016).

31. Shen, Q. *et al.* NAT10, a nucleolar protein, localizes to the midbody and regulates cytokinesis and acetylation of microtubules. *Experimental Cell Research* **315,** 1653–1667 (2009).

32. Liu, H. *et al.* DNA damage induces N-acetyltransferase NAT10 gene expression through transcriptional activation. *Mol. Cell. Biochem.* **300,** 249–258 (2007).

33. Gordon, L. B., Rothman, F. G., López-Otín, C. & Misteli, T. Progeria: A Paradigmfor Translational Medicine. *Cell* **156,** 400–407 (2014).

34. Gordon, L. B. *PRF By The Numbers (The Progeria Research Foundation)*. (2013).

35. Hutchinson-Gilford Progeria Syndrome and its Relevance to Cardiovascular Diseases and Normal Aging. *Biomedical and Environmental Sciences* **26,** 382–389 (2013).

36. Musich, P. R. & Zou, Y. Genomic instability and DNA damage responses in progeria arising from defective maturation of prelamin A. *Aging (Albany NY)* **1,** 28–37 (2009).

37. Duveau, F. & Félix, M.-A. Role of Pleiotropy in the Evolution of a Cryptic Developmental Variation in Caenorhabditis elegans. *PLOS Biology* **10,** e1001230 (2012).

## End Notes

**Acknowledgements.** We thank all members of the Steve Jackson laboratory for help and support, and Dr Carlos Lopez-Otin for sharing his *Lmna*$^{G609G}$ mouse model with us. Research in the Jackson laboratory is funded by Cancer Research UK (CRUK) program grant C6/A11224 and a Wellcome Trust Investigator Award (206388/Z/17/Z). Institute core funding is provided by CRUK (C6946/A14492) and the Wellcome Trust (WT092096). D.L was funded by a Project Grant from the Medical Research Council, UK MR/L019116/1. Research in the D.J.A. laboratory is supported by CRUK and the Wellcome Trust. Research in the R. R. laboratory is supported by the European Research Council (Grant N° 647973), and the Emergence Ville de Paris Program. M.D. was supported by the European Research Council grant DDREAM. Some data in this publication form part of the subject matter of patent WO 2015/150824. The funders had no role in study design, data collection and analysis, decision to publish or preparation of the manuscript.

**Author contributions.** GB, SPJ and DL coordinated the study and wrote the manuscript. DL conceptualized the study, performed the human and mouse derived cell culture, prepared the small molecule doses for animal gavage, generated immunofluorescence and western blots with help from MD and analyzed the related data. GB analyzed the survival and fertility data, performed the heart rate measurements, kyphotic index measurements, and sperm counts as well as mouse primary cell line derivations. GB helped with tissue collection throughout the study. AB genotyped all the mice in this study, did all the mouse protein extractions and analyzed the weighting data. CC did the Remodelin and Remodelin fluor gavages and mouse weighting with covering help from other mouse facility staff and supervised daily by AK that throughout the study helped with end-point criteria assessment making sure

consistency is achieved. MA performed the RNAseq analysis and pathway analysis with help from GB. NG performed the RNA extractions and did the qPCR analysis with help from GB. CJL and JKW supervised the phenotypic analysis; CJL assembled all the phenotypic pipeline raw data produced by Sanger Mouse Genetics Project (Carl Shannon; Mark Sanderson; Amy Gates; Joshua Dench, Valerie Vancollie, Catherine McCarthy, Selina Person, Emma Cambridge, Christopher Isherwood, Heather Wilson and Evelyn Grau) that performed all the pipeline phenotypic measurements in this study as well as the IVF analysis. NK performed the statistical analysis on the phenotypic pipeline data and helped throughout with all the statistical analysis in the paper. NK had an important contribution to manuscript material and methods writing. JM and AJ performed the pathologic staining and assessments. DC performed the meiotic spreads analysis. RR designed and synthesized the small molecules Remodelin and Remodelin Fluor used in the study. DJA helped supervise all the mouse work. SPJ supervised the work. All authors commented and edited the manuscript and figures.

**Conflict of interest.** The authors declare they have no conflict of interest.

## Figure Legends

**Fig. 1: Oral administration of Remodelin enhances health of progeria mice. a, b**: Cells were treated with vehicle or with 1μM Remodelin for 7 days. **a** Left: Representative immunofluorescence images of skin fibroblasts from *Lmna*$^{G609G/G609G}$ mice showing accumulation of the DNA double strand break marker γH2AX (green) and characteristic nuclear shape abnormalities observed by DAPI staining. All images were acquired with the same microscope intensity settings. Scale bar 20μm. Right: Quantification of γH2AX positive cells and cells with misshapen nuclei (>100 cells/n=3 independent cell lines; mean ± s.d.; ns = not significant; *p<0.05, **p<0.01, ***p<0.001, two-tailed Student's t-test). **b** Western blotting analysis of γH2AX levels (quantified in the right panel) in skin fibroblasts from the indicated genotypes. **c** and **d** Pharmacokinetic analyses of Remodelin in mice treated *via* oral (PO; n=3) or intravenous (IV; n=3) delivery; mean ± s.e.m. F: absolute bioavailability (%). **e** Tissues were collected after 2 weeks' of daily PO administration of the indicated Remodelin concentration, and 1 hour after the last dosing. Remodelin was quantified by mass spectrometry in heart and skeletal muscle (n=3); mean ± s.e.m. **f** Survival based on 20% body weight loss showing a 25% increase in Kaplan–Meier area under the curve in Remodelin treated *Lmna*$^{G609G/G609G}$ mice as compared to vehicle-treated mice (see Supplementary Table 3); (*Log-rank Mantel-Cox test; Chi-square 5.992). Due to animal welfare regulations, mice had to be sacrificed when they had lost 20% of their body weight compared to their individual weight maxima (end-point). However, at this defined end-point, Remodelin-treated mice displayed considerably better health compared to vehicle-treated controls (see supplementary movies and pathology assessments in Figure 2).

**Fig. 2: Remodelin ameliorates cardiac and other pathologies of HGPS mice.** Pathological staining in panels **a-d** was carried out on materials from endpoint mice (presented in Fig. 1**e**) of indicated genotypes (n=6 per genotype) treated with vehicle or Remodelin 100mg per kg per day (for detailed ages of the mice, see Supplementary Table 4). All images are representative (scale bar 50μm) and the correspondent bar graph quantifications are presented (mean ± s.e.m.; individual data points represented; ns = not significant; *p<0.05, **p<0.01, ***p<0.001, ****p<0.0001 two-tailed Student's t-test). In WT mice, Remodelin treatment has no significant effect as compared to vehicle treatment, and for simplicity these animals have been pooled in one group; the individual comparison is presented in Supplementary Fig. 2b. **a** Hematoxilin and eosin (H&E) staining of skin, indicating fat layer thickness (vertical bars indicate the fat layer) and showing amelioration of the fat layer thickness upon Remodelin treatment in HGPS mice. **b** H&E staining of heart aorta, indicating increased adventitial width in the HGPS mice as compared to WT controls, which is rescued by Remodelin treatment (arrowheads demarcate the aorta and vertical bars the adventitia). **c** DAPI staining of heart aorta, showing a decreased number of nuclei in the HGPS mice, rescued by Remodelin treatment (dotted white lines delineate the aorta edges). **d** Smooth muscle actin (SMA) staining (green) of heart aorta sections showing loss of integrity of the artery wall in HGPS mice, improved by Remodelin treatment (dotted white lines delineate the aorta). **e** and **f** Representative western blotting analysis of representative heart (**e**) and lung (**f**) tissues from endpoint mice, showing that Remodelin decreased γH2AX levels in *Lmna*$^{G609G/G609G}$ tissues (see quantification below each Western blot, relative to total H2AX levels). Western blots were performed more than once on n≥4/group.

**Fig. 3: Engineering and characterization of a *Nat10*$^{+/-}$ mouse model. a** Number of observed embryos (E14.5) and mice (21 days) compared to expected numbers (Mendelian frequencies) (*p<0.01; Chi-square analysis). **b** and **c** *Nat10*$^{+/-}$ mice display ~50% reduction in *Nat10* transcript level (**b**- each bar indicates individual mice ± SD of n=5 technical replicates/mouse) or protein expression in the indicated tissues (**c**- representative western blot; blots have been performed more than once on n≥3 mice) and quantification is presented on the right panel, relative to the Actin levels. **d** Heatmap of genes differentially expressed in the heart of *Nat10*$^{+/-}$ mice compared to wild-type from RNAseq analysis (n=2/genotype).

**Fig. 4: Genetic depletion of *Nat10* enhances health of *Lmna*$^{G609G}$ mice. a** *Lmna*$^{G609G/G609G}$*Nat10*$^{+/-}$ mice show 21% increased median age at endpoint compared to *Lmna*$^{G609G/G609G}$ (103 days versus 85 days respective median age at endpoint; based on mice being terminated upon reaching 20% body weight loss); (** Log-rank, Mantel-Cox test; Chi-square 32.61; also see Table S3). **b-d** Appearance (**b**) of back curvature (**c**) in *Lmna*$^{G609G/G609G}$ is delayed by *Nat10* depletion as observed by images of terminal mice and X-rays from 9 week-old females, and quantified (kyphotic index) over time (**d**) (mean ± SEM; individual data points represented; mixed model analysis shows a significant difference between *Lmna*$^{G609G/G609G}$*Nat10*$^{+/+}$ and *Lmna*$^{G609G/G609G}$*Nat10*$^{+/-}$ genotypes **p=0.01; raw data and extended conclusions and statistics are presented in Suppl. Data file 3). **e** Progressive heart function failure observed in *Lmna*$^{G609G/G609G}$ mice over time is delayed by *Nat10* depletion, as observed by heart rate measurements at indicated times (mean ± SEM; individual data points represented; mixed model analysis shows a significant difference between *Lmna*$^{G609G/G609G}$*Nat10*$^{+/+}$ and *Lmna*$^{G609G/G609G}$*Nat10*$^{+/-}$ genotypes ***p=0.004; raw data

and extended conclusions and statistics are presented in Data file S3). **f** RNA expression from heart tissues shows decreased *p21* expression in *Lmna*$^{G609G/G609G}$*Nat10*$^{+/-}$ compared to controls (mean ± SEM; ns = not significant, *p<0.05 two-tailed Student's t-test; individual data points represented). **g** *Lmna*$^{+/G609G}$*Nat10*$^{+/-}$ mice show 17% increased median age at endpoint compared to *Lmna*$^{+/G609G}$ (333 days versus 285 days respective median age at endpoint; based on mice being terminated upon reaching 20% body weight loss); (*Log-rank, Mantel-Cox test; Chi-square 4.98; also see Table S3) and more than 90 days between the longest lived *Lmna*$^{+/G609G}$*Nat10*$^{+/-}$ and the longest lived *Lmna*$^{+/G609G}$ mouse.

**Fig. 5: Identification of readouts for *Nat10* inhibition in cells and tissues. a and b** Representative images of western blots showing that 1μM Remodelin treatment for 7 days decreases the high α-tubulin K40 acetylation in HGPS-patient derived cells (**a**) and mouse tissues (**b**). In panel (**b**), NAT10 chemical (lane 3) or genetic (lane 4) inhibition reverses high α-tubulin K40 acetylation levels in heart tissues from indicated mice; * indicates a cross-reacting band. We note that the ratio between Lamin A and C appears to vary between tissues. All western blotting experiments were performed at least three times independently (n≥3/genotype). **c** Representative immunofluorescence images of acetyl-α-tubulin K40 in HGPS-patient derived cells as compared to matching healthy fibroblasts. Scale bar 20μm. K40 α-tubulin acetylation (red) is increased in the HGPS-patient derived cells and decreased upon Remodelin treatment. **d** Representative immunofluorescence images (left) and quantification (right) of acetyl-α-tubulin K40 in aortas of terminal mice of the indicated genotypes and treatments. Scale bar 10μm. K40 α-tubulin acetylation (green; white arrowheads point to example of cells that show increased K40 acetylation) is increased in

*Lmna*$^{G609G/G609G}$ mice and significantly decreased in such mice upon Remodelin treatment (n=3; mean ± SD; individual data points represented; ns = not significant, *p<0.05; **p<0.01, ***p<0.001; two-tailed Student's t-test). For better visualization, these are higher magnification snap-shots (red dotted squares) from images in Supplementary Fig. 9d. Quantification was performed on full size aorta images from n=3 independent mice.

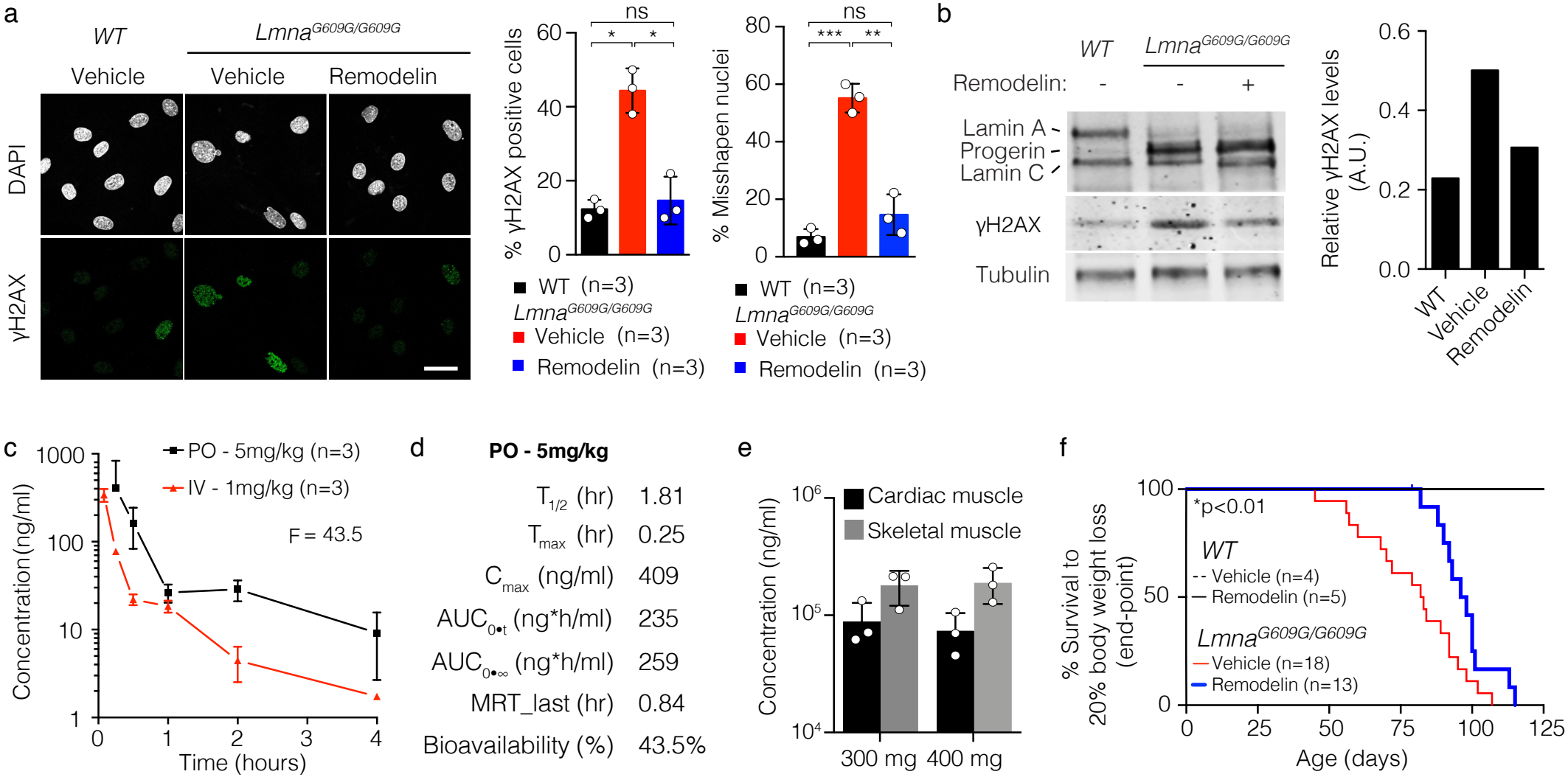
a
WT
Lmna G609G/G609G
Vehicle
Vehicle
Remodelin
DAPI
γH2AX
% γH2AX positive cells
ns
* *
WT (n=3)
Lmna G609G/G609G
Vehicle (n=3)
Remodelin (n=3)
% Misshapen nuclei
ns
*** **
WT (n=3)
Lmna G609G/G609G
Vehicle (n=3)
Remodelin (n=3)
b
WT
Lmna G609G/G609G
Remodelin: - - +
Lamin A
Progerin
Lamin C
γH2AX
Tubulin
Relative γH2AX levels (A.U.)
WT
Vehicle
Remodelin
c
PO - 5mg/kg (n=3)
IV - 1mg/kg (n=3)
F = 43.5
Concentration (ng/ml)
Time (hours)
d
PO - 5mg/kg
T1/2 (hr) 1.81
Tmax (hr) 0.25
Cmax (ng/ml) 409
AUC0•t (ng*h/ml) 235
AUC0•∞ (ng*h/ml) 259
MRT_last (hr) 0.84
Bioavailability (%) 43.5%
e
Cardiac muscle
Skeletal muscle
Concentration (ng/ml)
300 mg
400 mg
f
*p<0.01
WT
Vehicle (n=4)
Remodelin (n=5)
Lmna G609G/G609G
Vehicle (n=18)
Remodelin (n=13)
% Survival to 20% body weight loss (end-point)
Age (days)

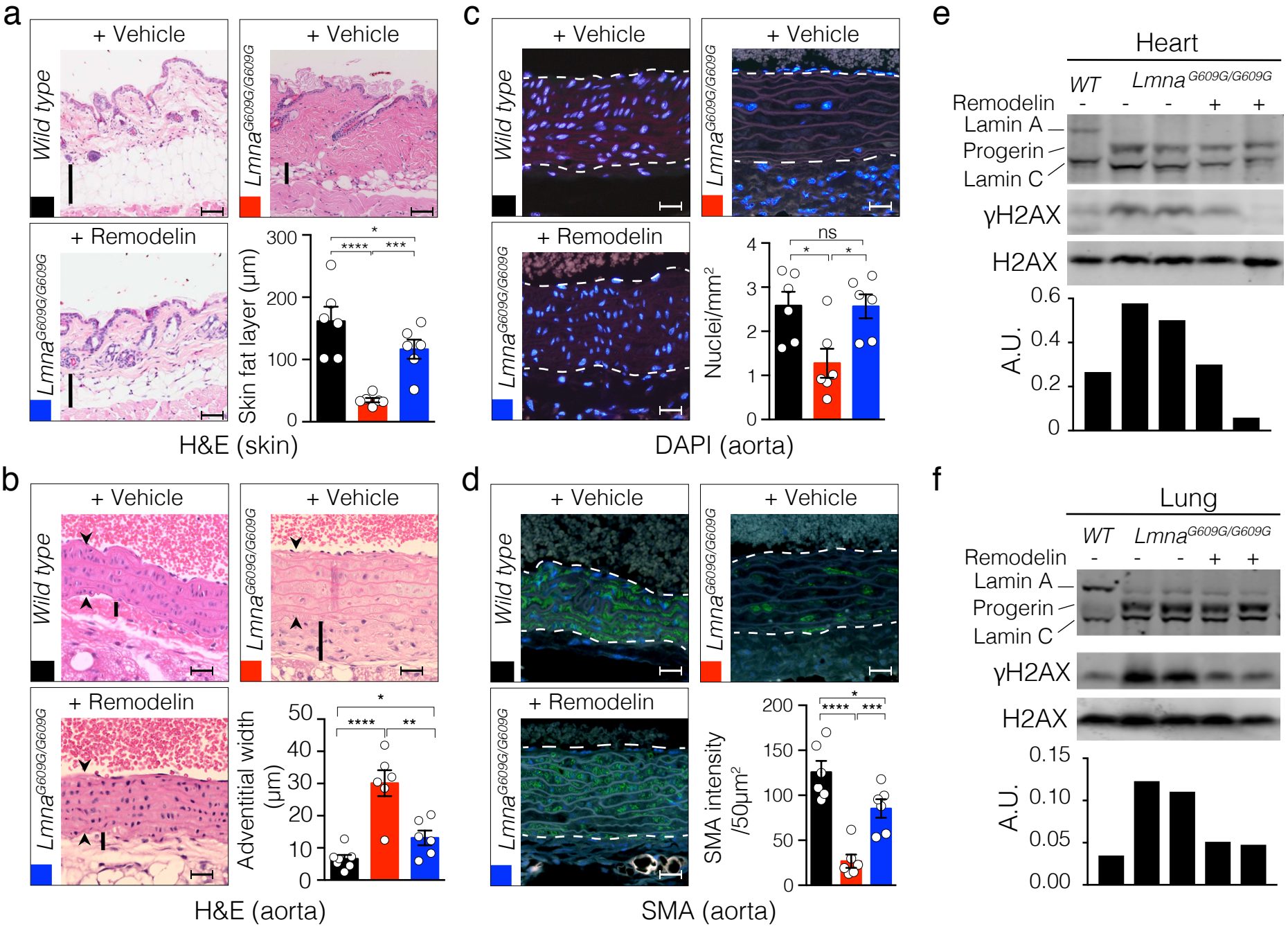
a
+ Vehicle
+ Vehicle
Wild type
Lmna G609G/G609G
+ Remodelin
Lmna G609G/G609G
Skin fat layer (µm)
300
200
100
0
*
****
***
H&E (skin)
c
+ Vehicle
+ Vehicle
Wild type
Lmna G609G/G609G
+ Remodelin
Lmna G609G/G609G
Nuclei/mm2
4
3
2
1
0
ns
*
*
DAPI (aorta)
e
Heart
WT
Lmna G609G/G609G
Remodelin
- - - + +
Lamin A
Progerin
Lamin C
γH2AX
H2AX
A.U.
0.6
0.4
0.2
0
b
+ Vehicle
+ Vehicle
Wild type
Lmna G609G/G609G
+ Remodelin
Lmna G609G/G609G
Adventitial width (µm)
50
40
30
20
10
0
*
****
**
H&E (aorta)
d
+ Vehicle
+ Vehicle
Wild type
Lmna G609G/G609G
+ Remodelin
Lmna G609G/G609G
SMA intensity /50µm2
200
150
100
50
0
*
****
***
SMA (aorta)
f
Lung
WT
Lmna G609G/G609G
Remodelin
- - - + +
Lamin A
Progerin
Lamin C
γH2AX
H2AX
A.U.
0.15
0.10
0.05
0.00

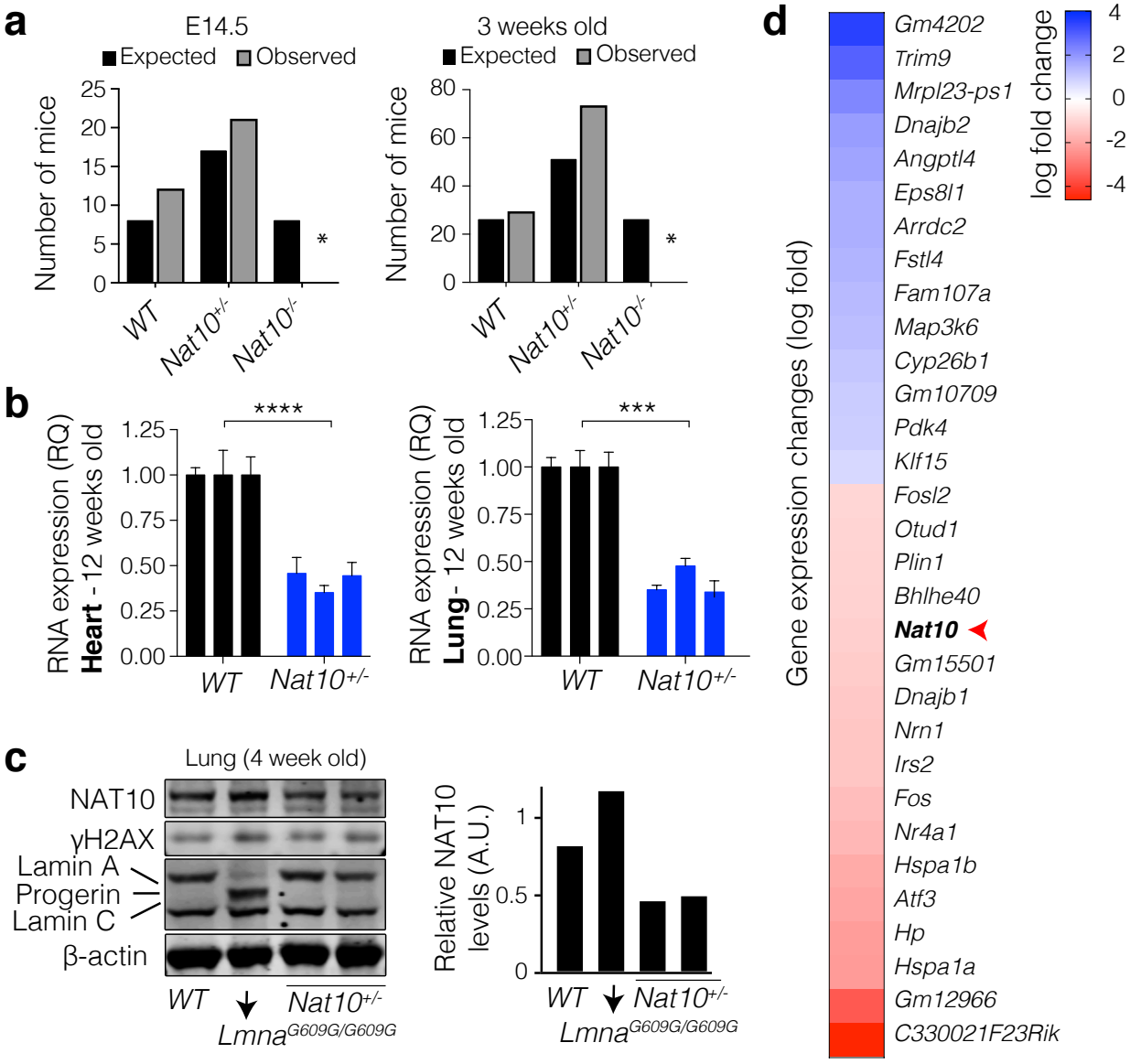
a
E14.5
Expected
Observed
Number of mice
25
20
15
10
5
0
*
WT
Nat10+/-
Nat10-/-
3 weeks old
Expected
Observed
Number of mice
80
60
40
20
0
*
WT
Nat10+/-
Nat10-/-
b
RNA expression (RQ)
Heart - 12 weeks old
****
1.25
1.00
0.75
0.50
0.25
0.00
WT
Nat10+/-
RNA expression (RQ)
Lung - 12 weeks old
***
1.25
1.00
0.75
0.50
0.25
0.00
WT
Nat10+/-
c
Lung (4 week old)
NAT10
γH2AX
Lamin A
Progerin
Lamin C
β-actin
WT
Nat10+/-
LmnaG609G/G609G
Relative NAT10 levels (A.U.)
1
0.5
0
WT
Nat10+/-
LmnaG609G/G609G
d
Gene expression changes (log fold)
Gm4202
Trim9
Mrpl23-ps1
Dnajb2
Angptl4
Eps8l1
Arrdc2
Fstl4
Fam107a
Map3k6
Cyp26b1
Gm10709
Pdk4
Klf15
Fosl2
Otud1
Plin1
Bhlhe40
Nat10
Gm15501
Dnajb1
Nrn1
Irs2
Fos
Nr4a1
Hspa1b
Atf3
Hp
Hspa1a
Gm12966
C330021F23Rik
log fold change
4
2
0
-2
-4

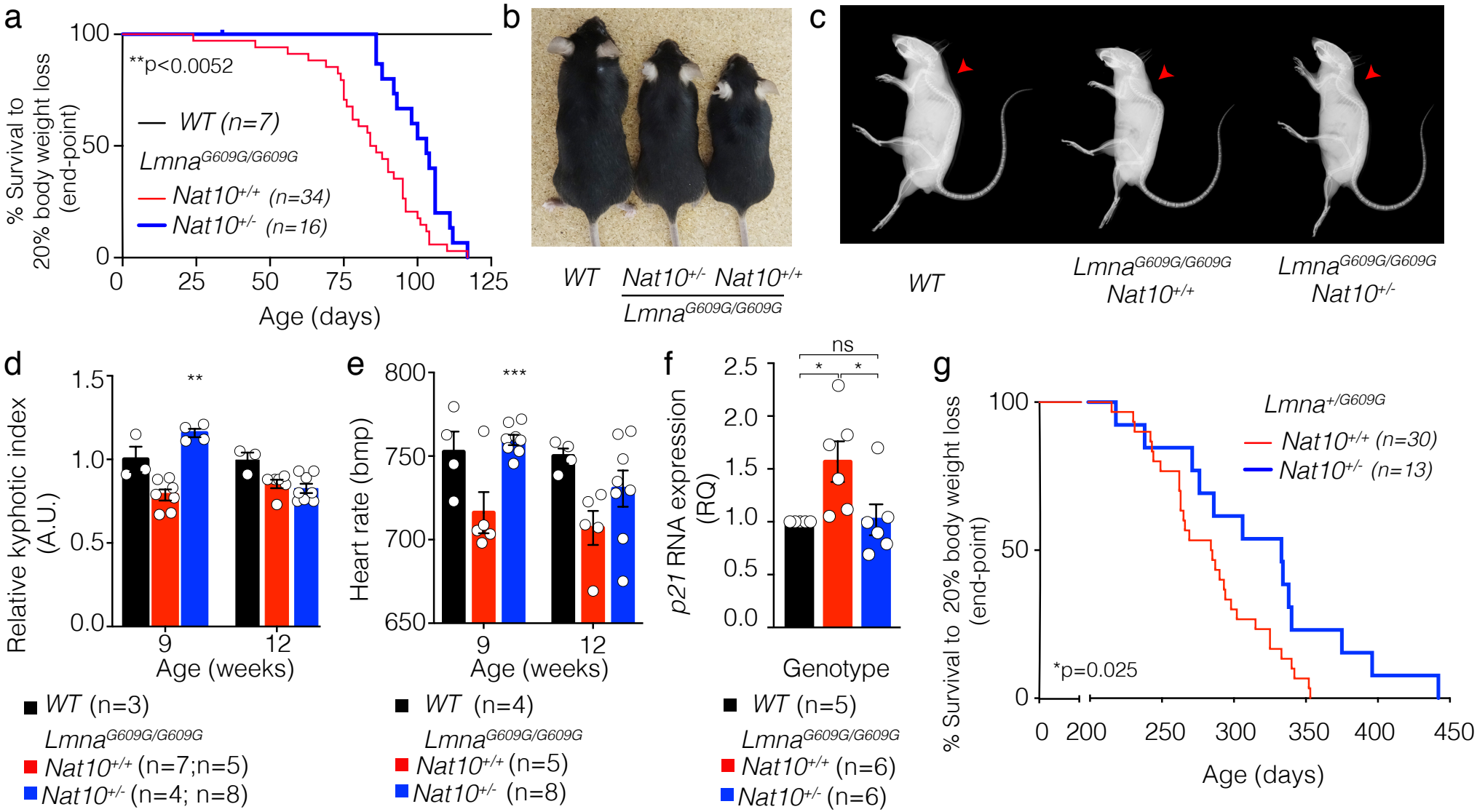
a
% Survival to 20% body weight loss (end-point)
100
50
0
**p<0.0052
WT (n=7)
Lmna G609G/G609G
Nat10 +/+ (n=34)
Nat10 +/- (n=16)
0
25
50
75
100
125
Age (days)
b
WT
Nat10 +/-
Nat10 +/+
Lmna G609G/G609G
c
WT
Lmna G609G/G609G Nat10 +/+
Lmna G609G/G609G Nat10 +/-
d
Relative kyphotic index (A.U.)
1.5
1.0
0.5
0.0
**
9
12
Age (weeks)
WT (n=3)
Lmna G609G/G609G
Nat10 +/+ (n=7;n=5)
Nat10 +/- (n=4; n=8)
e
Heart rate (bmp)
800
750
700
650
***
9
12
Age (weeks)
WT (n=4)
Lmna G609G/G609G
Nat10 +/+ (n=5)
Nat10 +/- (n=8)
f
p21 RNA expression (RQ)
2.5
2.0
1.5
1.0
0.5
0.0
ns
*
*
Genotype
WT (n=5)
Lmna G609G/G609G
Nat10 +/+ (n=6)
Nat10 +/- (n=6)
g
% Survival to 20% body weight loss (end-point)
100
50
0
Lmna +/G609G
Nat10 +/+ (n=30)
Nat10 +/- (n=13)
*p=0.025
0
200
250
300
350
400
450
Age (days)

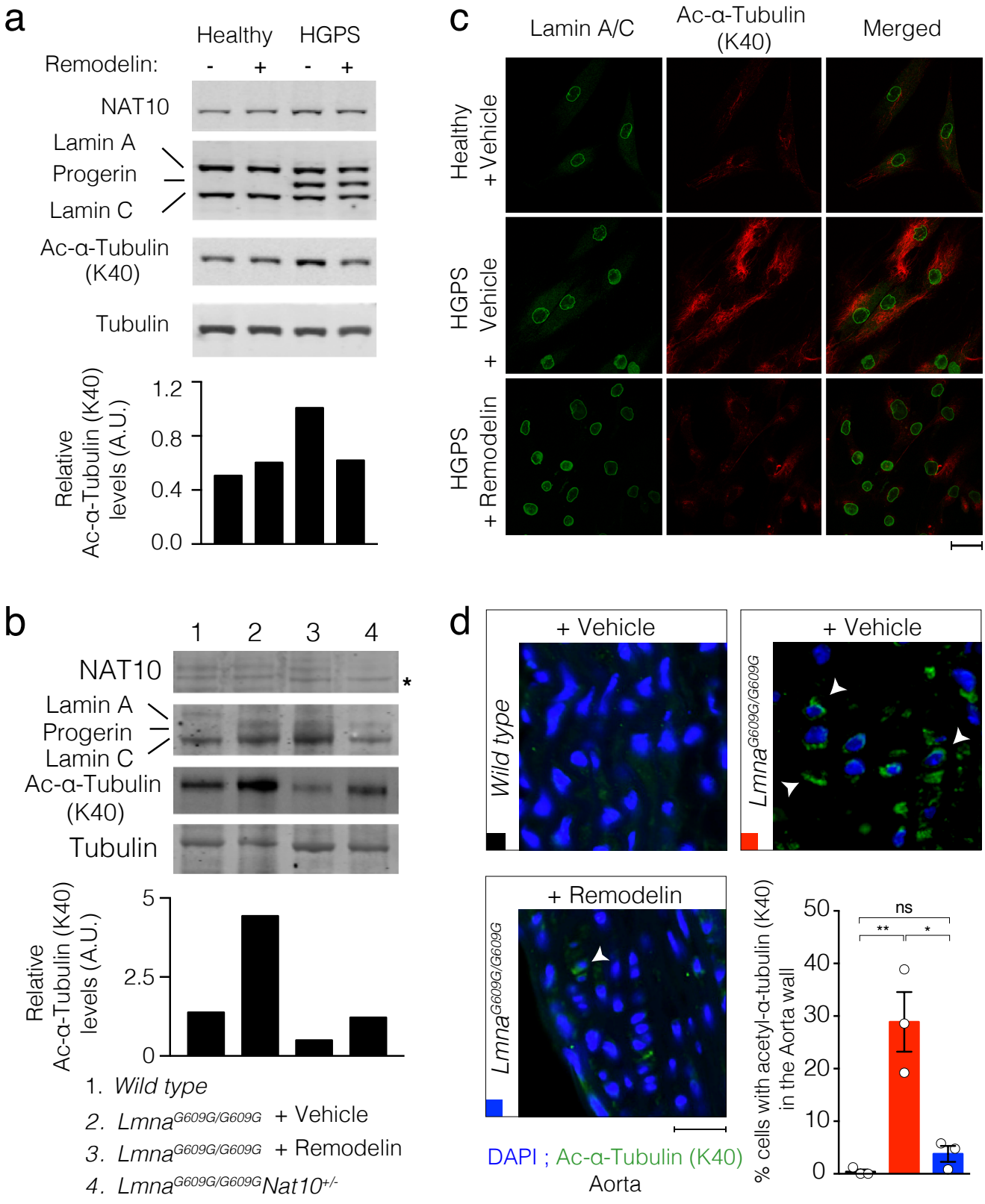
a
Healthy
HGPS
Remodelin:
- + - +
NAT10
Lamin A
Progerin
Lamin C
Ac-α-Tubulin (K40)
Tubulin
Relative Ac-α-Tubulin (K40) levels (A.U.)
1.2
0.8
0.4
0.0
b
1 2 3 4
NAT10
Lamin A
Progerin
Lamin C
Ac-α-Tubulin (K40)
Tubulin
*
Relative Ac-α-Tubulin (K40) levels (A.U.)
5
2.5
0
1. Wild type
2. Lmna G609G/G609G + Vehicle
3. Lmna G609G/G609G + Remodelin
4. Lmna G609G/G609G Nat10 +/-
c
Lamin A/C
Ac-α-Tubulin (K40)
Merged
Healthy + Vehicle
HGPS + Vehicle
HGPS + Remodelin
d
+ Vehicle
Wild type
+ Vehicle
Lmna G609G/G609G
+ Remodelin
Lmna G609G/G609G
DAPI ; Ac-α-Tubulin (K40)
Aorta
% cells with acetyl-α-tubulin (K40) in the Aorta wall
50
40
30
20
10
0
ns
**
*

Supplementary Materials for

# Targeting of NAT10 enhances healthspan and lifespan in a mouse model of human accelerated aging syndrome

Gabriel Balmus[1,2,9], Delphine Larrieu[1,8,9,10], Ana C Barros[1,2], Casey Collins[2], Monica Abrudan[2], Mukerrem Demir[1], Nicola J Geisler[1,2], Christopher J. Lelliott[2], Jacqueline K. White[2], Natasha A Karp[2,3], James Atkinson[3], Andrea Kirton[2], Matt Jacobsen[3], Dean Clift[4], Sanger Mouse Genetics Project[2], Raphael Rodriguez[5,6,7], David J Adams[2], Stephen P Jackson[1,10]

1. The Wellcome Trust/Cancer Research UK Gurdon Institute and Department of Biochemistry, University of Cambridge, United Kingdom.

2. The Wellcome Trust Sanger Institute, Hinxton, Cambridge, United Kingdom.

3. AstraZeneca, Cambridge, United Kingdom.

4. Laboratory of Molecular Biology, Cambridge, United Kingdom.

5. Institut Curie, PSL Research University, Paris Cedex 05, France.

6. CNRS UMR3666, 75005 Paris, France.

7. INSERM U1143, 75005 Paris, France.

8. Current address: Cambridge Institute for Medical Research, University of Cambridge, United Kingdom.

9. G.B. and D.L. contributed equally to this work

10. To whom correspondence may be addressed: s.jackson@gurdon.cam.ac.uk and dl437@cam.ac.uk

**Supplementary Materials file includes:**

Supplementary Materials and Methods

Tables S1 to S3

Supplementary Figures S1 to S10

Captions for Supplementary Data files S1 to S5

Captions for Movies S1 to S3

**Other Supplementary Materials for this manuscript includes the following:**

Supplementary Data files S1 to S5

Movies S1 to S3

## Materials and Methods

**Synthesis of Remodelin and derivatives.** All solvents and reagents were purified using standard techniques or used as supplied from commercial sources (Sigma-Aldrich). NMR spectra were acquired on a Bruker 500 MHz instrument using deuterated solvents at 300 K. Notation for the $^{1}$H NMR spectral splitting patterns includes: singlet (s), doublet (d), triplet (t), broad (br) and multiplet/overlapping peaks (m). Signals are quoted as values in ppm and coupling constants (J) are quoted in Hertz. Mass spectra were recorded on a Micromass® Q-Tof (ESI) spectrometer.

General procedure: The appropriate ketone or aldehyde was dissolved in isopropanol at a final concentration of 0.5 M and refluxed for 24h in the presence of an equimolar amount of thiosemicarbazide. The corresponding thiosemicarbazones were isolated by filtration and recrystallized from hot ethanol. Equimolar amounts of thiosemicarbazones and the desired haloketones were stirred at room temperature in isopropanol overnight at a final concentration of 0.2 M. The resulting products were recrystallized from hot ethanol several times to yield pure products and were used without further purification.

***4-(4-cyanophenyl)-2-(2-cyclopentylidenehydrazinyl)thiazole ( Remodelin).*** 2-cyclopentylidenehydrazine-1-carbothioamide (1 g, 4.46 mmol) and 2-bromo-4'-cyanoacetophenone (700 mg, 4.45 mmol) were stirred overnight in 12 ml of isopropanol at room temperature. The precipitate was filtered and recrystallized from hot ethanol to yield the hydrobromide salt of the desired compound (559 mg,

1.98 mmol, 45%) as light yellow needles. $^{1}$H NMR (500 MHz, $CDCl_3$): δ 12.11 (br s), 7.84 (d, J = 9.0 Hz, 2H), 7.81 (d, J = 9.0 Hz, 2H), 6.84 (s, 1H), 2.61 (t, J = 9.0 Hz, 2H), 2.51 (t, J = 9.0 Hz, 2H), 1.94–1.80 (m, 4H); $^{13}$C NMR (125 MHz, $CDCl_3$): δ 173.8, 169.5, 138.8, 133.5, 131.3, 126.3, 118.0, 114.1, 103.8, 33.7, 31.2, 25.2, 25.0; HRMS (m/z): $[M]^+$ calcd. for $C_{15}H_{15}N_4S$, 283.1009; found, 283.1017. Molecule **4** was resuspended in DMSO at 10mg/ml.

***4-(4-trifluoromethylphenyl)-2-(2-cyclopentylidenehydrazinyl)thiazole (Remodelin Fluor).*** 2-cyclopentylidenehydrazine-1-carbothioamide (3.0 g, 18.7 mmol) and 2-bromo-4'-(trifluoromethyl)acetophenone (5.0 g, 18.7 mmol) were stirred in isopropanol (150 mL) at r.t. for 24 h. The precipitate was filtered and recrystallized three times from hot ethanol to yield the hydrobromide salt of Remodelin Fluor as bright yellow needles (1.5 g, 3.7 mmol, 20%). 1H NMR (300 MHz, CDCl3) δ 11.12 (br s, 2H), 7.80 (d, *J* = 8.5 Hz, 2H), 7.65 (d, *J* = 8.5 Hz, 2H), 6.87 (s, 1H), 2.53 (t, *J* = 7.0 Hz, 2H), 2.47 (t, *J* = 7.0 Hz, 2H), 1.93–1.75 (m, 4H). 13C NMR (75 MHz, CDCl3) δ 171.9, 169.4, 140.3, 131.8 (q, *J* = 32.0 Hz), 131.6, 126.5 (br q, *J* = 3.5 Hz, 2C), 126.1 (2C), 123.7 (q, *J* = 274.0 Hz), 103.5, 33.5, 30.6, 25.1, 24.9. HRMS (m/z): [M+H]+ calculated for C15H15F3N3S, 326.0933; found, 326.0950. See Fig. S2*A* for the synthesis reaction.

**Animals - ethical information**

**Studies at Wellcome Trust Sanger Institute (WTSI).** The care and use of all mice used to generate data for this protocol was carried out in accordance with UK Home Office regulations, UK Animals (Scientific Procedures) Act of 2013 under

UK Home Office licenses which approved this which were reviewed regularly by the WTSI Animal Welfare and Ethical Review Board.

**Studies at Crown Biosciences.** The protocol and any amendment(s) or procedures involving the care and use of animals in this study were reviewed and approved by the Institutional Animal Care and Use Committee (IACUC) of CrownBio. During the study, the care and use of animals were conducted in accordance with the regulations of the Association for Assessment and Accreditation of Laboratory Animal Care (AAALAC AN-1308-017-66).

**Animals – experimental details**

**Studies at WTSI. Engineering of the *Nat10*$^{tm1a(KOMP)Wtsi}$ (*Nat10*$^{+/-}$) mice.** Mice carrying the knockout-first conditional-ready allele *Nat10*$^{tm1a(KOMP)Wtsi}$ (abbreviated to *Nat10*$^{tm1a}$) were generated on a C57BL/6N background as part of the Sanger Mouse Genetics Project (MGP). Detailed description of the Sanger Mouse Genetics Project methodology has been reported (Skarnes et al. 2011). Briefly, a promoter-containing cassette (L1L2_ Bact_P) was introduced upstream of the critical *Nat10* exon 4 at position 103754720 of Chromosome 2, Build GRCm38. The vector containing *Nat10*$^{tm1a}$ was electroporated into C57BL/6N derived JM8A3.N1 ES cells. Correct ES cell gene targeting was confirmed by long-range PCR and quantitative PCR. Targeted ES cells were microinjected into blastocysts and used to generate chimeras. Germ-line transmission was confirmed by genotyping PCR analyses (http://www.knockoutmouse.org/kb/25/). Mice obtained from heterozygous intercross were genotyped for the *Nat10*$^{tm1a}$ allele by PCR.

***Lmna$^{G609G}$* and *Lmna$^{G609G}$ Nat10$^{+/-}$* mice.** *Lmna$^{G609G}$* (C57BL/6N) mice were imported from the laboratory of Carlos-Lopez Otin (1) and re-derived on the line C57BL/6NTac at the Wellcome Trust Sanger Institute (WTSI). Mouse genotyping was performed from tail biopsies using a protocol already described (1). *Nat10* KO mice were generated in the C57BL/6NTac background as part of the Mouse Genetics Project at the WTSI (2). The double mutant combinations were maintained on the same C57BL/6NTac background. Experimental animals were maintained under close supervision following the following protocol. Upon weaning *Lmna$^{G609G/G609G}$* homozygous animals and littermate *Lmna$^{+/+}$* wild-type (WT) controls were set up in experimental cohorts and weighed weekly. WT and mutant experimental animals were housed together randomly in multiple cages to reduce cage bias. Treatment and weight measurements were carried out by the mouse facility technicians blinded of the scientific background or goals of the experiment. When animals would reach 10% body weight (BW) loss they would be weighed every other day and wet pellets provided on the floor daily. Upon 15% BW loss animals would be weighed and monitored daily and culled when they passed over 19% BW loss. A number of male mice of the Lmna$^{G609G/G609G}$ genotype have presented with penile prolapse and upon detection they have been culled and indicated as incidence of penile prolapse (Figure 3B). Over the course of the study 3 mice of the Lmna$^{G609G/G609G}$ genotype have been found dead. No drug or naïve test was performed prior to treatment or testing. Animals have been euthanized by CO2 inhalation followed by cervical dislocation. WTSI facility runs periodic health reports that indicate that the mice were free of known viral, bacterial and parasitic

pathogens. For analysis of embryonic development of Nat10 KO mice, timed matings were performed at noon and the day of vaginal plug detection was defined as embryonic day E0.5. Movies and pictures were made using a Sony Cyber-shot DSC-HX10V GPS camera. Mouse health evaluation was performed by trained technicians using established protocols (3).

**Studies at Crown Biosciences.** For testing drug bioavailability pilot studies have been performed on 7 weeks old C57BL/6 mice, weighing between 18.8-19.9g. The mice were ordered from Shanghai Laboratory Animal Center (SLAC, Shanghai, China). Animals have been euthanized by CO2 inhalation followed by cervical dislocation.

**Animals – housing and husbandry**

**Studies at WTSI.** Our mice are maintained in a specific pathogen-free unit on a 12-h light: 12-h dark cycle with lights off at 19:30 and no twilight period. The ambient temperature is 21 ± 2 °C, and the humidity is 55 ± 10%. Mice are housed using a stocking density of 3–5 mice per cage (overall dimensions of caging: 365 × 207 × 140 mm (length × width × height), floor area 530 cm2) in individually ventilated caging (Tecniplast, Sealsafe 1284L) receiving 60 air changes per hour. In addition to Aspen bedding substrate, standard environmental enrichment of two Nestlets, a cardboard fun tunnel and three wooden chew blocks are provided. Mice were given water and diet (Teklad Global 18% Protein Rodent Diet/Envigo) ad libitum.

**Studies at Crown Biosciences.** Mice were housed at an average temperature of 23.5ºC with a 7:00 am - 19:00 pm light and 19:00 pm – 7:00 am (next day) darkness cycle in polysulfone IVC cages (3 mice/cage; 325 mm x 210 mm x 180 mm). Mice were fed $Co^{60}$ irradiation sterilized dry granule mouse diet. Animals had free access to food and water during the entire study period. Mice had no drug or test naïve prior to treatment.

**Small molecule dosing.** Remodelin and Remodelin Fluor were dissolved in a solution of 20% DMSO, 65% (45% 2-Hydroxypropyl-b-cyclodextrin solution, H5784 Sigma Aldrich) and 15% Tween 80 (P8074 Sigma Aldrich). The "vehicle" treated animals were given this solution alone, without Remodelin. Remodelin and Remodelin Fluor were administered daily by oral gavage at 100mg/kg/day and 50mg/kg/day respectively (defined as non-toxic doses in toxicity studies), from day 21 and until culled. Dosing needle - Instech FTP-20-30 Plastic feeding tubes, 20ga X 30mm 1 ml syringes and 20ga dosing needles were used as they are appropriate for the volume to be administered and for the size of the mice. During each dosing session, the vehicle only was administered to each animal in the control group before administering Remodelin to each animal in the treated group to avoid cross-contamination. Body weights were recorded for each mouse before dosing and the dose volume was calculated according to the body weight. The mice were restrained by scruffing the back of the neck, the dosing needle was presented through the mouth down into the oesophagus in a smooth motion. Once *in situ,* the dose (calculated to a 100 to 200µl volume) was administered to the mouse. Additional food was moistened and added to the floor of each cage to facilitate

food consumption following the dosing procedure. The end-point criteria were represented by 20% body weight loss, mice that were found death or moribund and mice that presented with penile prolapse, a distinctive clinical phenotype for the progeric male mice. All animals were used to represent the survival curves; n=1 Remodelin treated *Lmna*$^{G609G/G609G}$ mouse presented with hemangioma at 79 days of age and was censored into the survival analysis. Treatment and weight measurements were carried out by the mouse facility technicians blinded of the scientific background or goals of the experiment. The comparison between *Lmna*$^{G609G/G609G}$ vehicle and *Lmna*$^{G609G/G609G}$ no treatment showed no significant difference (p=0.56). We utilized an informally method of randomizing within each batch to assign mice to treatment using mouse database ID. Mice were used from multiple cages and litters.

**Assessment of Remodelin toxicity *in vivo*.** Remodelin toxicity was assessed by Crown Biosciences on twelve 6 weeks old C57BL/6N female mice, with a body weight of 20g on average (animal supplier: Shanghai Laboratory Animal Center (SLAC, Shanghai, China): see Table S2.

LC/MS/MS method was used to assess Remodelin concentration in plasma. Minimum of 6 standards with lowest limit of quantification (LLOQ) <3 ng/mL and minimum of 5 standards back were calculated to within ±20% of their nominal concentrations. Total 6 quality control (QC) samples at 3 concentrations (Low, Mid and High) were included in sample runs with a minimum of 4 QC back calculated to within ±20% of their nominal concentrations.

**Pharmacokinetics Evaluation of Remodelin in ICR Mouse *via* IV and PO administration.** The pharmacokinetics of Remodelin was assessed by Crown Bioscience. The administration of Remodelin and sample collection in each study group are shown in the following experimental design table (IV= intravenous; P.O.= *per os* (by mouth)). Animals were randomly assigned to groups: see Table S3. Before grouping and treatment, all animals were weighed, and assigned into groups using randomized block based on their body weight. Within each block, experimental animals were randomly assigned to the different groups. Randomized block design was used to assign experimental animals to ensure that each animal has the same probability of being assigned to any given treatment groups and therefore minimise systematic error. Animals showing obvious signs of severe distress and/or pain were humanely sacrificed. In case of following situations, the animals were euthanized: Animal has lost significant body mass (>20%, emaciated). The animals found to be having other severe health problems, i.e., prolonged diarrhea, persistent anorexia, lethargy or failure to respond to gentle stimuli, labored respiration, or that cannot get to adequate food or water, etc., were removed from the study and sacrificed (n=3; sub-cutaneous administration; data not shown). LC/MS/MS method development was used to assess test compound in plasma. Minimum of 6 standards with LLOQ <3 ng/mL and minimum of 5 standards back were calculated to within ±20% of their nominal concentrations. Total 6 QC samples at 3 concentrations (Low, Mid and High) will be included in sample runs with a minimum of 4 QC back were calculated to within ±20% of their

nominal concentrations. Plasma samples were analysed following the above criteria.

**Immunoblotting.** Mice were euthanized by $CO_2$ inhalation followed by cervical dislocation. Mouse tissues were snap-frozen in liquid $N_2$ and immediately stored at -80ºC. 40µl/g of protein extraction buffer (50 mM Tris pH 7.5, 150 mM NaCl, 0.1% NP-40, 0.5% CHAPS, 5 mM MgCl2, 10% glycerol, MilliQ distilled water) or Laemmli Buffer (S3401 SIGMA). Mini-protease and mini-phosphatase tablet was added to each sample in conjunction with a stainless-steel bead (7mm; QUIAGEN) and physical disrupted using the TissueLyser LT (QIAGEN), in 2x5 min cycles with 5 min rest on ice in between. After removing the stainless-steel bead, the lysates were sonicated using the BioruptorTM Next Gen (Diagenode), 2x20 min cycles (30 sec on, 30 sec off), and a 20 min rest period on ice in between. The tissue derbies were separated from the protein content by centrifugation using a bench Eppendorf centrifuge 5417R (Eppendorf) for 30 min, at 4ºC and 16400 rpm. The quantity of protein was measured using PierceTM BCA protein assay kit (Thermo Scientific) and Muiltyskan GO (Thermo Scientific) at an absorbance of 562 nm. Before loading, lysates were diluted with a solution of 0.01% bromophenol blue and 200 mM DTT and boiled for 5 min at 95°C. Proteins from individual mice/cell lines were resolved by SDS-PAGE on 4-12% gradient gels (NUPAGE, Life Sciences) and transferred onto nitrocellulose membrane (Protran; Whatman). Secondary antibodies conjugated to IRDye 800CW were from LI-COR Biosciences. Western blotting shown are representative of 3 repeats. Detection and quantification was performed with an imager (Odyssey; LI-COR Biosciences).

**Cell lines.** Normal skin primary fibroblasts GM03440 and Hutchinson Gilford Progeria Syndrome (HGPS) skin primary fibroblasts AG11513 were purchased from Coriell Cell Repositories and used between passage number 9-17. Cells were grown in Dulbecco's modified Eagle medium (DMEM, Sigma-Aldrich) supplemented with 10% fetal bovine serum (BioSera), 2mM L-glutamine, 100U per ml penicillin, 100 µg $ml^{-1}$ streptomycin. All cell lines have been tested for mycoplasma contamination using Charles River Mycoplasma Testing Services.

**Immunofluorescence.** Isolation and culture of adult mouse fibroblasts from skin and lungs was performed using an established protocol, as previously described (4). Cells were washed with PBS and fixed for 10 min with 4% PFA in PBS. Cells were permeabilised for 5 min with PBS/0.2% Triton X-100, and blocked with PBS/0.2% Tween 20 (PBS-T) containing 5% BSA. Coverslips were incubated for 1 h with primary antibodies and for 30 min with appropriate secondary antibodies coupled to Alexa Fluor 488 or 594 fluorophores (Life Technologies), before being incubated with 2µg/ml DAPI. Pictures were acquired with a FluoView 1000 confocal microscope (Olympus) and images were quantified using ImageJ. All the immunofluorescence experiments were performed at least 3 times independently and the pictures shown in the figures are representative images of the at least 3 experiments.

**Histology and immunohistochemistry.** All major organs were isolated following euthanasia and then fixed in 10% formalin overnight. The second day the fixed organs were transferred to 70% ethanol, were placed in cassettes, embedded in

paraffin and serial 5 μm sections were collected on Superfrost Plus slides (Fisher) using a Leica microdissection system (LMD7000). Hematoxilin and eosin (HE) and immunohistochemistry staining were performed as previously described (5). The organs were examined for abnormalities by a Board Certified Veterinary Pathologist (MJ). Sections of heart containing aortic outflow, pulmonary artery and myocardium were stained using a primary antibody against alpha smooth muscle actin (SMA-Sigma Aldrich Cat No: A2547 1:1000) and secondary antibody (Alexa 488 Life Technologies at 1:100). The heart sections were also stained using DAPI alone and with an antibody against Acetyl α Tubulin (K40) (5335 Cell Signalling). Representative histology images were obtained from whole slide images scanned on a Hamamatsu NanoZoomer in brightfield and fluorescence modes. The thickness of the subcutaneous fat layer in the skin and nuclei number in the aorta were measured using whole slide images and the Hamamatsu NDP view software at a magnification of ×200 (resolution of 0.45μm per pixel). The skin (always the same region/the flanks) and aorta regions for analysis were identified by a pathologist (MJ) and manually annotated using the HALO image analysis software (Indica Labs). The cells inside these annotated regions were identified and counted using the HALO software CytoNuclear v1.5 algorithm, the output of cell density (cells/$mm^2$) was used to differentiate between the treatment groups. SMA intensity quantification was performed using ImageJ.

**Oocyte culture and immunofluorescence.** Oocytes were isolated from ovaries of 8-week old C57BL/6N female mice and cultured in M2 medium covered by mineral oil at 37ºC. Isolated oocytes were maintained in prophase arrest by

addition of 250 μM dbcAMP (Sigma; D0627). To induce resumption of meiosis, oocytes were released into dbcAMP-free medium. For immunofluorescence, oocytes were fixed for 30 min at 37ºC in 100 mM HEPES (pH 7; titrated with KOH), 50 mM EGTA (pH 7; titrated with KOH), 2% formaldehyde (methanol free) and 0.2% Triton X-100. Fixed oocytes were incubated in PBS with 0.1% Triton X-100 overnight at 4ºC. Antibody incubations were performed in PBS, 3% BSA and 0.1% Triton X-100. Primary antibodies used were rat anti-Nup98 (Abcam, ab50610; 1:100) and rat anti-tyrosinated-α-tubulin (YOL1/34, AbD Serotec; 1:3000). Secondary antibodies used were Alexa-Fluor-488-labelled anti-rat (Molecular Probes; 1:400). DNA was stained with 5 mg $ml^{-1}$ Hoechst 33342 (Molecular Probes). Images were acquired with a Zeiss LSM710 microscope equipped with a 63x C-Apochromat 1.2 NA water-immersion objective.

**Generation of oocytes and *in-vitro* fertilization.** Three 4 to 5 week old C57BL/6NTac females per sperm sample were super-ovulated by intraperitoneal (IP) injection of 5IU of pregnant mare's serum at 17:00 hrs (on a 12hr light/dark cycle, on at 07:00/off at 19:00) followed 48hrs later by an IP injection of 5IU human chorionic gonadotrophin. Oviducts were dissected at approximately 07:50am on the day of the in-vitro fertilization (IVF), and cumulus-oocyte complexes were transferred into the IVF fertilization dish containing human tubal fluid (HTF)+ glutathione (GSH). An aliquot of 20μl of sperm from the pre-incubation dish was then added to the fertilization dish. After allowing 3-4 hours for fertilization to occur the embryos were washed and cultured overnight in HTF at 37$^{o}$C, 5% $CO_2$ in air.

**Antibodies.** Antibodies used in this study are: Lamin A/C (sc-6215 Santa-Cruz), NAT10 (13365-1-AP ProteinTech Europe), γH2AX (05-636 Millipore), H2AX (ab11175 Abcam), β Actin (ab8226, Abcam), Acetyl α Tubulin (K40) (5335 Cell Signalling), α Tubulin (T9026 Sigma-Aldrich), Nup98 (Abcam, ab50610) and tyrosinated-α-tubulin (YOL1/34, AbD Serotec).

**High throughput phenotyping screen.** The high-throughput phenotyping, is based on a pipeline concept where a mouse is characterized by a series of standardized and validated set of tests underpinned by standard operating procedures. The phenotyping tests chosen cover a variety of disease-related and biological systems, including the metabolic, cardiovascular, bone, neurological and behavioral, sensory and hematological systems and clinical chemistry. The data were obtained as detailed previously (2) following the standard operating procedures at IMPReSS (www.mousephenotype.org/impress). Factors thought to affect the variables were standardized as far as possible. Where standardization was not possible, steps were taken to reduce potential bias. For example, at WTSI the impact of different people completing the experiment was minimized ("minimized operator") as defined in the Mouse Experimental Design Ontology (MEDO) (6) as "The process by which steps are taken to minimize the potential differences in the effector by training and monitoring of operator." (http://bioportal.bioontology.org/ontologies/MEDO/?p=summary). The data captured with the MEDO ontology can be accessed at http://www.mousephenotype.org/about-impc/arrive-guidelines. Pre-set reasons are established for QC failures (e.g. insufficient sample) and detailed within

IMPRESS (www.mousephenotype.org/impress) providing standardized options as agreed by area experts as to when data can be discarded. Data can only be QC failed from the dataset if clear technical reasons can be found for a measurement being an outlier. Reasons are provided and this is tracked within the database.

Phenotyping data are collected at regular intervals on age-matched wildtype (control) mice of equivalent genetic backgrounds. Cohorts of at least seven homozygote mice of each sex per knockout line were generated. If no homozygotes were obtained from 28 or more offspring of heterozygote intercrosses, the line was deemed homozygous lethal. Similarly, if less than 13% of the pups resulting from intercrossing were homozygous, the line was judged as being homozygous sub-viable. In such circumstances, heterozygote mice were committed to the phenotyping pipelines.

The random allocation of mice to experimental group (wildtype versus knockout) was driven by Mendelian Inheritance. Reflecting the high-throughput nature of the phenotyping pipeline, blinding to the identity of knockout lines during phenotyping was not employed as the cage cards include genotype information, though with a high throughput environment without a defined hypothesis, the potential bias is minimized. The individual mouse was considered the experimental unit within the studies. Further detailed experimental design information (e.g. exact definition of a control animal) is captured by with a standardized ontology as detailed in Karp *et al* (6) and is available from the IMPC portal

(http://www.mousephenotype.org/about-impc/arrive-guidelines). For each line, n≥5 mice/genotype were studied.

**Comparison between Wild-type, *Lmna*$^{G609G/G609G}$, and *Lmna*$^{G609G/G609G}$*Nat10*$^{+/-}$.** Mutant mice at 9 or 12 weeks of age were analyzed in separate groups (n≥3 for each sex/genotype). Prior to entering this workflow, due to the progeria phenotype, mice were assessed for adverse health and welfare to ensure that mice were in a suitable condition for analysis. No mice were excluded from study on this basis. Mice were anaesthetized with 110mg/kg body weight ketamine and 11mg/kg body weight xylazine given intraperitoneally. Mice were then imaged sequentially with three modalities, high resolution X-Ray imaging (MX-20, Faxitron, Tucson, AZ), Dual-energy X-ray Absorptiometry for body composition (Piximus II, GE Healthcare, Hatfield, UK) and with light photography for imaging of dysmorphology. A whole-body lateral image using the MX-20 was collected for the analysis of spinal curvature by trained persons using a standard defined position to minimize inconsistencies between mice. Following this and still while under anaesthesia, blood collection was performed to obtain samples for plasma chemistry and haematological analysis *via* the retro-orbital route using capillary tubes (cat. no. 078042; Scientific Laboratory Supplies). Mice were then culled by cervical dislocation and heart removal, followed by removal of other organs for analysis. During this series of procedures, the experimenters collecting images and blood samples were not blinded from the genotypes of the mice. However, the analysis of the blood parameters was blinded and uploaded onto a database. The kyphosis index (KY) was calculated as the ratio between a line drawn between the caudal

margin of the last cervical vertebra to the caudal margin of the sixth lumbar vertebra and a line perpendicular to this from the dorsal edge of the vertebra at the point of greatest curvature as previously described (7). For the data collected on the back curvature, a multilevel regression model was performed using R (package:nlme version 3.1). A model (Eq. 1), treating genotype, sex and age as fixed effects whilst the repeat measure nature of the dataset was accounted for by treating mouse as a random effect, was fitted to the data. The genotype effect was tested and contrasts used to directly compare *Lmna*$^{G609G/G609G}$ and *Lmna*$^{G609G/G609G}$*Nat10*$^{+/-}$ mice if the genotype effect was significant. For the hypothesis test of primary interest, the impact of genotype, p-values were adjusted to account for the multiple comparisons completed to control the false discovery rate to 0.05. Visual inspection of the data was used to assess whether variance was equal and no outliers were present thus ensuring the assumptions of the model were met.

Y ~ Genotype + Sex + Age + (1|Mouse) [Eq. 1]

For the survival analysis, the end-point criteria were represented by 20% body weight loss, mice that were found death or moribund and mice that presented with penile prolapse, a distinctive clinical phenotype for the progeric male mice. All animals were used to represent the survival curves; one *Lmna*$^{G609G/G609G}$*Nat*$^{10+/-}$ was reported by the technician staff with a swollen abdomen at 32 days of age and requested to be culled. The mouse was active and within the weight range for the

age. No abnormality was found at necropsy but because it was culled for other reasons than end-point criteria it was censored from the analysis.

**Statistical analysis**. For all analyses, the individual mouse was considered the experimental unit within the studies. Survival distributions of the different cohorts was plotted using the Kaplan–Meier estimator and statistical analysis was performed using log-rank (Mantel-Cox) test. For survival analysis we have completed power calculations for a large size effect and with an n of 10/group. We could detect a 0% to 60% change in survival after treatment, 91% of the time (power of Fisher Exact test, 0.91). To meet the assumption of this statistical method, censoring of an individual mouse could only occur when the culling of a mouse was not related to the genotype/assessed-phenotype (e.g. fight wound leading to overt clinical presentation).

***Nat10*$^{+/-}$ and *Lmna*$^{G609G}$ high-throughput phenotyping data**. Knockout data collected across multiple batches were compared to a year's worth of control data collected on mice from the same genetic background. For the continuous data, an iterative top down mixed modelling strategy fitting equation 1 was performed as described (8) using PhenStat, an R package version 2.6.0 (9) freely available from Bioconductor (10) The package's mixed model framework was used as default except the argument equationType was set to withoutWeight and dataPointsThreshold was set to 2. The model optimisation implemented will adjust for unequal variances. The genotype contribution test p value was adjusted for multiple testing to control the false discovery rate to 5%. This statistical method

has been studied through simulations and resampling studies (11) and found to be robust and reliable with a multi-batch workflow, where the knockout mice are split into multiple phenotyping batches.

$$Y \sim Genotype + Sex + Genotype*Sex + (1|Batch) \quad [Eq. 2]$$

For the categorical data, a Fisher Exact Test was fitted comparing the proportions seen between wildtype and knockout mice for each sex independently using PhenStat FE Framework with the default settings. This simple method is appropriate for categorical phenotyping data as discussed in Karp et al. 2012 (8). The minimum p value returned from the two tests for a variable was adjusted for multiple testing to control the false discovery rate to 5%. The number of caudal vertebrae were recoded to a categorical variable by classifying mice with less than 28 vertebrae as “low”, those with greater than 29 as “high” and all others as “normal”. For ABR data, the knockout dataset was smaller with only four data points for each variable, therefore to meet the assumption of the test, the data was analysed using a reference range plus methodology (9) which calls a significant phenotype when the majority of animals lie outside the natural variation seen in the control animals. The implementation within PhenStat RR framework is based on classifying the analysable variable values as high, normal, low based on the natural variation seen within the control data and comparing the proportions seen with a Fisher Exact Test. The minimum p value returned from the two tests (1:

increase in high classification and 2: increase in low classification) for a variable was adjusted for multiple testing to control the false discovery rate to 5%.

As a high throughput program with many variables and multiple analysis tools, a single power calculation would not help; instead, the pipeline has been developed through empirically selecting a workflow which has historically given hits at a rate that would be cost effective for the program.

**Comparison between Wild-type, *Lmna*$^{G609G/G609G}$, and *Lmna*$^{G609G/G609G}$*Nat10*$^{+/-}$**

Mixed model data analysis was performed using R (package: nlme version 3.1). An iterative top down modelling strategy was implemented starting with the fully loaded model (Eq. 2). For the Origins of Bone and Cartilage Disease (OBCD) screen (12), where only one sex was collected, Eq. 3 details the starting model. The final model was selected by first selecting a structure for the random effects, then a covariance structure for the residual, and then the model reduced by removing non-significant fixed effects. Then the genotype effect was tested, model diagnostics assessed and contrasts used to directly compare *Lmna*$^{G609G/G609G}$ and *Lmna*$^{G609G/G609G}$*Nat10*$^{+/-}$ mice if the genotype effect was significant. During the model building stage, the hypotheses were tested with a threshold of $p<0.05$. For the hypothesis test of primary interest, the impact of genotype, p-values were adjusted to account for the multiple comparisons completed to control the false discovery rate to 0.05. The difficulty associated with the breeding and viability challenged the production of these mice for the array of phenotyping used in this paper. 136 mating pairs were set up over more than 3 years that generated 181

*Lmna*$^{G609G}$ homozygous (single or *Nat10* double-mutant) mice that were used at specific ages together with littermate controls. The *n* was thus limited by breeding constraint and we have used n>5.

Y=Genotype + Age + (1|Batch)  [Eq. 3]

**Heart rate comparison.** Heart measurements were performed using the ecgTUNNEL (emka TECHNOLOGIES), a noninvasive ECG system, using the manufacturer recommendations as previously described (13). All ECG recording sessions were performed during daytime and the data analyzed using the *iox2*, data acquisition and analysis software (emka TECHNOLOGIES). For data acquisition, a series of repeated measurements were done on the same animal at each time-point and data for the same animal was collected over the different week intervals. For the data collected on the heart rate screen, a multilevel regression model was performed using R (package:nlme version 3.1). A model [Eq. 1], treating genotype, sex and age as fixed effects whilst the repeat measure nature of the dataset was accounted for by treating mouse as a random effect, was fitted to the data. The genotype effect was tested and contrasts used to directly compare *Lmna*$^{G609G/G609G}$ and *Lmna*$^{G609G/G609G}$*Nat10*$^{+/-}$ mice if the genotype effect was significant. For the hypothesis test of primary interest, the impact of genotype, p-values were adjusted to account for the multiple comparisons completed to control the false discovery rate to 0.05. Visual inspection of the data was used to assess whether variance was equal and no outliers were present thus ensuring the assumptions of the model were met.

**RNA extraction and qPCR analysis**. RNA was extracted from tissues from n>5 independent mice/group using the RNeasy fibrous tissue mini kit (50) (cat. No.7404; Qiagen) and quantified using the NanoDrop 1000 Spectrophotometer (Thermo Fisher Scientific). 2µg RNA/sample was used to produce cDNA using the High-Capacity RNA-to-cDNA kit (cat. No. 4387406; Applied Biosystems/Thermo Fisher Scientific). qPCR was carried out using the TaqMan system (Universal Master Mix II, with UNG, 4440038; Applied Biosystems/Thermo Fisher Scientific) on an Applied Biosystems Quant Studio 3 machine. n≥3 mice were used for each genotype, with 50ng cDNA for each sample run in triplicate or quadruplicate. Thermo Fisher Scientific *Nat10* (Mm00462302_m1) and *Cdkn1a/p21* (Mm00432448_m1) primers were used as experimental probes while *Gapdh* (Mm99999915_g1), *Actb* (Mm00607939_s1) and/or *Rn18s* (Mm03928990_g1) were used as endogenous controls. The Relative Standard Curve pre-set programme was used throughout and data analysis was performed using the Relative Quantification application, powered by the Thermo Fisher Scientific cloud platform. To account for technical replicates the mean value for a mouse was calculated and used for the statistical assessment. For each sample, data was normalized to the endogenous controls and represented as relative to the wildtype control. Data was evaluated by visual inspection and an F test of the variance was calculated in order to estimate normality and equal variance.

All graphs and part of the statistical analysis in the manuscript (Student's t-tests; Kaplan–Meier estimator and statistical analysis; Fishers exact test) were

generated and calculated using GraphPad Prism version 7.0a for Mac OS X, GraphPad Software, La Jolla California USA, www.graphpad.com.

**RNAseq data analysis.** RNA was extracted as described above and quality control assessed using the 2100 Bioanalyzer (Agilent Technologies). Because of financial constrains we used n=2 mice/group. Transcriptome data was obtained using paired end sequencing, with read lengths of 150 bp, on a NextSeq 500 machine. Trimmed reads were aligned using STAR aligner (version 2.4.2a) to the mouse genome assembly GRCm38. Normalisation of the read counts and differential expression analysis was performed using three commonly used software programmes: DeSeq2 (14), edgeR (15) and Cuffdiff 2 (16). Our conservative approach defined genes differentially expressed as those found to be in common between the results of at least two of the three software programmes mentioned above. The log-2 fold change in gene expression presented in Figure 2d and Figure 4e correspond to the log-2 fold change returned by DeSeq2. DeSeq2 and edgeR used as an input raw read counts produced by featureCounts from the Bioconductor (version 3.3) Rsubread package (14) in R version 3.3.1. For the DeSeq2 and edgeR analyses, we filtered out genes that had 0 or 1 read support across all samples. In the DeSeq2 differential expression analysis, we selected genes that were up or down regulated at a FDR lower than 0.1. In edgeR differential expression analysis, we selected genes up or down regulated with a p-value less than 0.05.

Gene ontology analysis was performed using the mouse genome informatics (MGI) visual annotation display (VLAD) (17). For the analysis of the biological term fold enrichment, a ratio between the frequency of genes in our set to frequency of genes in the whole genome was calculated (18).

**Data availability**. The mouse phenotypic data from the present manuscript are available in the supplementary Data files. Mouse phenotypic data will be available from IMPC (http://www.mousephenotype.org/). RNAseq data will be available from GEO public repository (https://www.ncbi.nlm.nih.gov/geo/).

**Supplementary figures**

**Fig. S1: Assessment of Remodelin effect *in vivo*. a** Toxicity assessment of Remodelin treatment on 6-week old C57BL/6N female mice. Group 1 (n=3) and 2 (n=3) were administered daily oral doses of the molecule (PO) as indicated, whereas group 3 (n=3) received Remodelin by subcutaneous injection (SC). No body weight loss or toxicity was observed on these regimes after 2 weeks of treatment. Error bars represent mean ± SD. **b** Long-term treatment of the *Lmna*$^{G609G/G609G}$ mice with Remodelin (100mg/kg/day) showed no drug-dependent body weight loss. Error bars represent mean ± SD. **c** The only observed side effect of Remodelin treatment (in all mice) was hair greying, appearing after several weeks' treatment in both WT (left mouse on each panel) and *Lmna*$^{G609G/G609G}$ mice (right mouse).

**Fig. S2: Identification of a more potent Remodelin analogue. a** Synthesis and chemical structure of Remodelin-fluor (left) and its analogue Remodelin (right). **b** Representative images of U2OS cells transfected with siRNA control (siCT) or siRNA against Lamin A/C (siLMNA). Nuclear shape was assessed by microscopy following DAPI staining of the nucleus. Remodelin-fluor showed increased potency in rescuing nuclear shape defects of Lamin A/C depleted cells (siLMNA) compared to Remodelin, and relative to the mock-treated cells (NT). **c** Representative images of mice treated with Remodelin-fluor. Long-term treatment of Remodelin-fluor at 50mg/kg/day only caused mild hair greying, specifically around the eyes, in all treated mice. **d** No drug dependent body weight loss or toxicity was observed on

50mg/kg/day of Remodelin-fluor treatment. Bars represent mean ± SD. **e** 50mg/kg/day oral Remodelin-fluor delivery led to a 30% Kaplan–Meier area under the curve lifespan increase in the *Lmna*$^{G609G/G609G}$ mice (see Table S1). Data for the vehicle-treated *Lmna*$^{G609G/G609G}$ mice (red line) was combined across experiments to allow comparison of survival and is also presented in Fig. 1**e**. ****Log-rank (Mantel-Cox) test comparison between *Lmna*$^{G609G/G609G}$ treated with Vehicle and *Lmna*$^{G609G/G609G}$ treated with Remodelin-fluor.

**Fig. S3: Remodelin improves the coronary pathology of HGPS mice. a** Representative images of hematoxilin and eosin (H&E) and smooth muscle actin (SMA) staining of heart sections representing coronary arteries (left panels; size bar 100μm) showing improved integrity of the artery wall in terminal *Lmna*$^{G609G/G609G}$ mice treated with Remodelin. Right panel: bar graph of the quantification of the SMA mean intensity/15μm$^2$ (mean ± SD; individual data points represented; ns = not significant; **p<0.01, ***p<0.001; two-tailed Student's t-test;). **b** Bar graph presenting the quantification of different indicated parameters in the aorta of the wild type (WT) Remodelin treated mice (n=3) vs. Vehicle treated mice (n=3). Remodelin has no significant effect (ns) as compared to Vehicle treatment and for simplicity in Figure 2 **a-d** the two have been pooled in one group (WT).

**Fig. S4: Engineering and characterisation of a *Nat10*$^{+/-}$ mouse model. a** Schematic representation of the gene-trap construct engineered to disrupt the *Nat10* gene. **b** The high throughput phenotyping pipeline had n≥337 WT female

mice, n≥337 WT male mice, n≥6 *Nat10*$^{+/-}$ female mice and n≥6 *Nat10*$^{+/-}$ male mice. The exact n number depended on the screen and can be seen in the respective excel data files (Supplementary Data file 1). Top: heat-map of adjusted p-value of the phenotypic outcomes of the represented assays in *Nat10*$^{+/-}$ mice compared to WT (red: significant parameter; blue: non-significant parameter). A significant difference in Klrg1 mature natural killer (Nk) cell number ($p^a$=0.002), Nk cell number ($p^a$=0.002) and neutrophil number ($p^a$=0.032) was observed specifically in the *Nat10*$^{+/-}$ males as compared to WT males, but not in females. Raw data are presented in Supplementary Data file 1. Bottom: zoom-in on significant parameters from the heat-map; Mchc (mean corpuscular hemoglobin concentration); AUC (weight area under curve); Mpv (mean platelet volume); Wbc (white blood cells). **c** Gene ontology analysis showing top scoring terms fold enrichment (false discovery rate: FDR<0.03; p<0.0005) from genes shown in Fig. 3**d**. The number of target genes in each category is shown.

**Fig. S5: Significant parameters from the heat-map of *Nat10*$^{+/-}$ mice.** From the mixed-model analysis, the estimated *Nat10*$^{+/-}$ genotype effect with 95% confidence intervals is shown for significant parameters. Unadjusted p values ($p^u$) and adjusted p-values ($p^a$) are represented. The high throughput phenotyping pipeline had n≥337 WT female mice, n≥337 WT male mice, n≥6 *Nat10*$^{+/-}$ female mice and n≥6 *Nat10*$^{+/-}$ male mice. The exact n number depended on the screen and can be seen in the respective excel data files (Supplementary Data file 1). **a** Some variables including weight area under the curve (AUC), lean mass, triglycerides, cholesterol, total food intake and fat mass showed differences in both males and

females. **b** Other variables including natural killer (NK) cells, neutrophils (number and percentage), mean corpuscular hemoglobin concentration (Mchc), potassium, monocytes comprising Ly6c negative ($Ly6c^-$) and Ly6c positive ($Ly6c^+$), mean platelet volume (Mpv), number of total T cells and white blood cells (Wbc) showed sexual dimorphism

**Fig. S6: *Lmna*$^{G609G/G609G}$ mice have overtly normal sperm and oocytes**. **a** Quantification of sperm cells in WT (n=3) and *Lmna*$^{G609G/G609G}$ (n=3) mice, showing no significant difference (p=0.09; two-tailed Student's t-test). Bar graphs representing mean ± SD. **b** Quantification of *in vitro* fertilisation potential of sperm from WT (n=2) and *Lmna*$^{G609G/G609G}$ (n=3) male mice using oocytes from WT mice and of oocytes from WT (n=4) and *Lmna*$^{G609G/G609G}$ (n=3) female mice using sperm from WT mice. Bar graphs representing mean ± standard deviation. Statistical significance was calculated using two-tailed Student's t-test. **c** and **d** Oocytes isolated from WT and *Lmna*$^{G609G/G609G}$ female mice are normal and show normal meiotic progression. Representative images show oocytes isolated from 8-week old WT and *Lmna*$^{G609G/G609G}$ female mice. The number of oocytes for each category is shown in bottom right-hand corner. Asterisk shows polar body. Scale bars, 20 μm. **e** NAT10 inhibition appeared to increase fertility in *Lmna*$^{G609G/G609G}$ mice but was not statistically significant due to low number of mice (p=0.29; two-tailed Fisher exact test).

**Fig. S7: Phenotypic characterisation of *Lmna*$^{+/G609G}$ mice.** The high throughput phenotyping pipeline had n≥300 WT female mice, n≥300 WT male mice, n≥5

*Lmna*$^{+/G609G}$ female mice and n≥5 *Lmna*$^{+/G609G}$ male mice. The exact n number depended on the screen and can be seen in the respective excel data files (Supplementary Data file 4). **a** Heat-map of adjusted p-values of the phenotypic outcomes from the high throughput phenotyping of in *Lmna*$^{+/G609G}$ mice compared to WT (red: significant parameter; blue: non-significant parameter). Raw data and statistical output are presented in Supplementary Data file 4. A zoom-in on significant parameters from the heat-map is shown. **b** From the mixed-model analysis**,** the estimated *Lmna*$^{+/G609G}$ genotype effect with 95% confidence intervals is shown for significant variables. Unadjusted p value ($p^u$) and adjusted p-values ($p^a$) are represented. Some variables including red cell distribution width, grip strength (all paws) and mean corpuscular volume showed sexual dimorphism (females-red bars; males blue bars). For the categorical parameters identified as significant using the Fisher exact test, such as humerus and tibia, X-ray imaging was used to distinguish between normal and abnormal morphology shown as a proportion plot.

**Fig. S8: *Nat10* depletion reduces back curvature in *Lmna*$^{+/G609G}$ mice. a** Images of two littermates at 250 days old. The *Lmna*$^{+/G609G}$ mouse displayed strong back curvature that was not observed in the *Lmna*$^{+/G609G}$*Nat10*$^{+/-}$ mouse. **b** X-ray of the indicated mouse genotypes. Arrows indicate back curvature, and show that in the heterozygous *Lmna*$^{+/G609G}$ mice, it is corrected by *Nat10* depletion. For WT mice, the occurrence of back curvature was rare, while we always see the phenotype in *Lmna*$^{+/G609G}$*Nat10*$^{+/+}$ *(n=30)* and delayed in *Lmna*$^{+/G609G}$ *Nat10*$^{+/-}$ *(n=13*).

**Fig. S9: Identification of signatures for *Nat10* inhibition in cells and *in vivo.*** **a** Heat map of genes differentially expressed in the heart of *Lmna*$^{G609G/G609G}$ mice (n=2) compared to wild-type (lane 1; n=2) and upon *Nat10* reduction (lane 2; n=2) or Remodelin treatment (lane 3; n=2). Asterisks indicate genes showing same expression level trends in both *Lmna*$^{G609G/G609G}$*Nat10*$^{+/-}$ and *Lmna*$^{G609G/G609G}$ Remodelin compared to *Lmna*$^{G609G/G609G}$. **b** Biological term analysis showing top-scoring terms fold-enrichment (FDR<0.03; p<0.0005) from the genes in row 1 of E. The number of target genes in each category is shown.

**Fig. S10: *Lmna*$^{G609G/G609G}$ mice display increased Lys-40 tubulin acetylation that is reduced upon Remodelin treatment**. **a** Representative western blot showing that NAT10 inhibition reverses the high tubulin acetylation levels in heart tissues from indicated mice and that decrease tubulin acetylation correlates with decreased gamma-H2AX phosphorylation. Western blots were repeated more than one time on multiple samples. **b** NAT10 inhibition restores normal levels of acetyl-tubulin, as observed by immunohistochemistry in heart sections of LmnaG609G/G609G mouse tissues; scale bars being 40μM and 50μM respectively. All the immunohistochemistry experiments were performed on independent mice (n≥3/genotype). **c** Representative immunofluorescence images of acetyl-tubulin (K40) in aortas; size bar 100μm; dotted white line delineates the aorta. Higher magnification snap-shots (red dotted squares) from these images are presented alongside quantification in Fig. 5**d**. **d** Representative immunofluorescence images (left) and quantification (right) of acetyl-tubulin (K40) in the coronary arteries of terminal mice of the indicated genotypes and treatment.

Size bar 50μm; dotted white line delineates the coronary. Lys-40 (K40) tubulin acetylation (green; white arrowheads point to cells that show increased K40-acetylation) is increased in the *Lmna*$^{G609G/G609G}$ mice that and significantly decreased upon Remodelin treatment (n=3 individual mice; mean ± SD; individual data points represented; ns = not significant, *p<0.05; **p<0.01, ***p<0.001; two-tailed Student's t-test).

**Supplementary data files**

**Data file 1:** Phenotypic analysis of *Nat10*$^{+/-}$ mice

**Data file 2:** RNAseq analysis of heart tissues from *Nat10*$^{+/-}$ mice

**Data file 3:** Phenotypic analysis of *Lmna*$^{G609G/G609G}$*Nat10*$^{+/-}$ and *Lmna*$^{+/G609G}$ *Nat10*$^{+/-}$mice at 9-12 weeks

**Data file 4:** Phenotypic analysis of *Lmna*$^{+/G609G}$ mice

**Data file 5:** RNAseq analysis of heart tissues from *Lmna*$^{G609G/G609G}$*Nat10*$^{+/-}$ mice and Remodelin treated *Lmna*$^{G609G/G609G}$ mice

**Supplementary movie captions**

**Movie 1:** *Lmna*$^{G609G/G609G}$ terminal mouse (20% body weight loss; 13-14 weeks old) showing premature ageing. The mouse presents rough hair coat, dirty incision, squinted eyes, hunched walk and moderate agitation, slight dehydration, pruritic and restless.

**Movie 2:** *Lmna*$^{G609G/G609G}$ and *Lmna*$^{G609G/G609G}$*Nat10*$^{+/-}$ age matched littermate controls at 13 weeks of age. *Lmna*$^{G609G/G609G}$*Nat10*$^{+/-}$ mouse (no weight loss; not terminal; right side at the beginning of the movie) is fitter than *Lmna*$^{G609G/G609G}$ mouse (20% body weight loss – terminal; left side at the beginning of the movie). While the *Lmna*$^{G609G/G609G}$ mouse is not well groomed, has an awkward gait, is slightly hunched and moves slowly, the *Lmna*$^{G609G/G609G}$*Nat10*$^{+/-}$ mouse is normal, well groomed, alert; active; in good condition and shows normal behavior.

**Movie 3:** Terminal *Lmna*$^{G609G/G609G}$*Nat10*$^{+/-}$ mice compared to WT littermate control. The *Lmna*$^{G609G/G609G}$*Nat10*$^{+/-}$ mice (two smaller mice; 20% body weight loss – terminal; upper and lower left side at the beginning of the movie) at 15-16 weeks of age show no other phenotype than body weight loss as compared to WT littermate control (one mouse; lower right side at the beginning of the movie). All mice are well groomed, alert; active; in good condition and show normal behavior.

## SUPPLEMENTARY REFERENCES


1 Osorio, F. G. *et al.* Splicing-directed therapy in a new mouse model of human accelerated aging. *Sci Transl Med* **3**, 106ra107, (2011).

2 White, J. K. *et al.* Genome-wide Generation and Systematic Phenotyping of Knockout Mice Reveals New Roles for Many Genes. *Cell* **154**, 452-464, (2013).

3 Burkholder, T., Foltz, C., Karlsson, E., Linton, C. G. & Smith, J. M. Health Evaluation of Experimental Laboratory Mice. *Curr Protoc Mouse Biol* **2**, 145-165, (2012).

4 Seluanov, A., Vaidya, A. & Gorbunova, V. Establishing primary adult fibroblast cultures from rodents. *J Vis Exp*, (2010).

5 Balmus, G. *et al.* HUS1 regulates in vivo responses to genotoxic chemotherapies. *Oncogene* **35**, 662-669, (2016).

6 Karp, N. A. *et al.* Applying the ARRIVE Guidelines to an In Vivo Database. *Plos Biol* **13**, (2015).

7 Laws, N. & Hoey, A. Progression of kyphosis in mdx mice. *J Appl Physiol (1985)* **97**, 1970-1977, (2004).

8 Karp, N. A., Melvin, D., Sanger Mouse Genetics, P. & Mott, R. F. Robust and sensitive analysis of mouse knockout phenotypes. *PLoS One* **7**, e52410, (2012).

9 Kurbatova, N., Mason, J. C., Morgan, H., Meehan, T. F. & Karp, N. A. PhenStat: A Tool Kit for Standardized Analysis of High Throughput Phenotypic Data. *PLoS One* **10**, e0131274, (2015).

10 Gentleman, R. C. *et al.* Bioconductor: open software development for computational biology and bioinformatics. *Genome Biol* **5**, R80, (2004).

11 Karp, N. A. *et al.* Impact of temporal variation on design and analysis of mouse knockout phenotyping studies. *PLoS One* **9**, e111239, (2014).

12 Freudenthal, B. *et al.* Rapid phenotyping of knockout mice to identify genetic determinants of bone strength. *J Endocrinol* **231**, R31-46, (2016).

13 Mongue-Din, H., Salmon, A., Fiszman, M. Y. & Fromes, Y. Non-invasive restrained ECG recording in conscious small rodents: a new tool for cardiac electrical activity investigation. *Pflugers Arch* **454**, 165-171, (2007).

14 Love, M. I., Huber, W. & Anders, S. Moderated estimation of fold change and dispersion for RNA-seq data with DESeq2. *Genome Biol* **15**, 550, (2014).

15 Robinson, M. D., McCarthy, D. J. & Smyth, G. K. edgeR: a Bioconductor package for differential expression analysis of digital gene expression data. *Bioinformatics* **26**, 139-140, (2010).

16 Trapnell, C. *et al.* Differential analysis of gene regulation at transcript resolution with RNA-seq. *Nature biotechnology* **31**, 46-53, (2013).

17 Richardson, J. E. & Bult, C. J. Visual annotation display (VLAD): a tool for finding functional themes in lists of genes. *Mamm Genome* **26**, 567-573, (2015).

18 Metzakopian, E. *et al.* Genome-wide characterization of Foxa2 targets reveals upregulation of floor plate genes and repression of ventrolateral genes in midbrain dopaminergic progenitors. *Development* **139**, 2625-2634, (2012).

## Supplementary Tables

### Table S1. Design table for the administration of the test articles and sample collection in each study group.

| Groups | n | Treatment | Dose (mg/kg) | Dosing Route | Schedule | Sample Collection | | | |
|---|---|---|---|---|---|---|---|---|---|
| | | | | | | Plasma (50µl) | Whole Blood | Heart | Muscle |
| 1 | 3 Female | Vehicle | 100 | PO | Single dose | 15min, 30min, 1h | NA | 1h* | 1h |
| 2 | 3 Female | Remodelin | 100 | PO | | 15min, 30min, 1h | NA | 1h | 1h |
| 3 | 3 Female | Vehicle | 100 | SC | | 15min, 30min, 1h | NA | 1h | 1h |
| 4 | 3 Female | Remodelin | 100 | SC | | 15min, 30min, 1h | NA | 1h | 1h |

Note: 1. n: animal number;
1. Dosing volume: adjust dosing volume based on body weight, SC (sub-cutaneous) group 10 ml/kg; PO (oral) group 10 ml
* One hour after treatment

**Table S2. Pharmacokinetics Evaluation of Remodelin *via* IV and PO administration.**

| Groups | n | Treatment | Dose (mg/kg) | Dosing Route | Schedule | Sample Collection | | | | Fasting |
|---|---|---|---|---|---|---|---|---|---|---|
| | | | | | | Plasma (50μl) | Whole Blood | Serum | Tissue | |
| 1 | 3 male | Remodelin | 1 | IV | Single dose | 5min, 2h | NA | NA | NA | Over night before the last dose |
| 2 | 3 male | | 1 | IV | | 15min, 4h, | NA | NA | NA | Over night before the last dose |
| 3 | 3 male | | 1 | IV | | 30min,8h, | NA | NA | NA | Over night before the last dose |
| 4 | 3 male | | 1 | IV | | 1h, 6h,24h | NA | NA | NA | Over night before the last dose |
| 5 | 3 male | | 5 | P.O. | | 15min, 4h | NA | NA | NA | Over night before the last dose |
| 6 | 3 male | | 5 | P.O. | | 30min, 6h, | NA | NA | NA | Over night before the last dose |
| 7 | 3 male | | 5 | P.O. | | 1h,8h, | NA | NA | NA | Over night before the last dose |
| 8 | 3 male | | 5 | P.O. | | 2h, 24h | NA | NA | NA | Over night before the last dose |
| 9 | 5 male | | NA | NA | | As much as possible | NA | NA | NA | Blank control |

Note: 1. n: animal number;
1. Dosing volume: adjust dosing volume based on body weight, IV (intra-venous) group ; PO (oral) group

## Table S3. Comparison of survival rates of mice in this study based on Kaplan-Meyer analysis

| Genotype comparisons | # deaths (censored) | Median survival (days) | Area Under the Curve (AUC) | % AUC | Log-rank Mantel-Cox test; Chi-square | df | P value |
|---|---|---|---|---|---|---|---|
| *Lmna*$^{G609G/G609G}$ *No treatment* | 33 (0) | 83.0 | 8015 | 100% | 0.32 | 1 | ns; 0.56 |
| *Lmna*$^{G609G/G609G}$ *Vector* | 18 (0) | 82.5 | 7644 | 95% | | | |
| *Lmna*$^{G609G/G609G}$ *Vector* | 18 (0) | 82.5 | 7644 | 100% | 5.99 | 1 | *; <0.014 |
| *Lmna*$^{G609G/G609G}$ *Remodelin* | 12 (1*) | 97.0 | 9575 | 125% | | | |
| *Lmna*$^{G609G/G609G}$ *Vector* | 18 (0) | 82.5 | 7644 | 100% | 17.6 | 1 | ****; <0.0001 |
| *Lmna*$^{G609G/G609G}$ *Remodelin Fluor* | 15 (0) | 107.0 | 9929 | 130% | | | |
| *Lmna*$^{G609G/G609G}$ *Nat10*$^{+/+}$ | 34 (0) | 85.0 | 8200 | 100% | 7.82 | 1 | **; <0.052 |
| *Lmna*$^{G609G/G609G}$ *Nat10*$^{+/-}$ | 15 (1**) | 103.0 | 9577 | 117% | | | |
| *Lmna*$^{+/G609G}$ *Nat10*$^{+/+}$ | 30 (0) | 284.5 | 27778 | 100% | 4.98 | 1 | *; <0.025 |
| *Lmna*$^{+/G609G}$ *Nat10*$^{+/-}$ | 13 (0) | 333.0 | 30246 | 109% | | | |

* this mouse was within normal weigh and was censored due to a health concern reported by the room technician as abnormal mass at 79 days of age; upon necropsy a hemangioma was found

** this mouse was within normal weigh and was censored due to a health concern reported by the room technician as swolen abdomen at 32 days of age; upon necropsy no abnormalities were found

## Supplementary Figures

Balmus et al. Figure S1

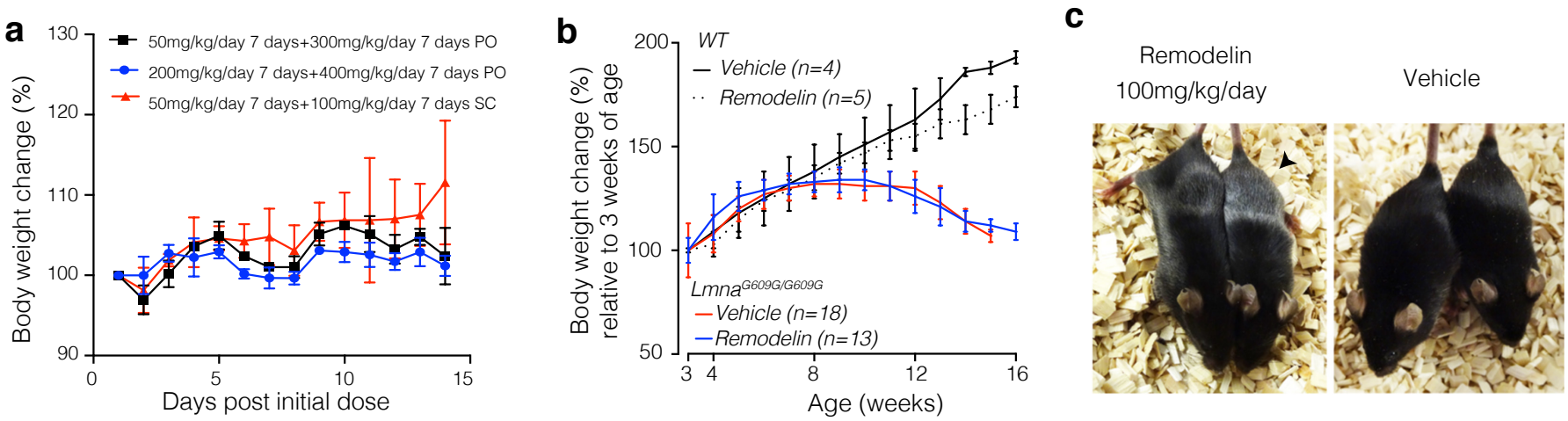

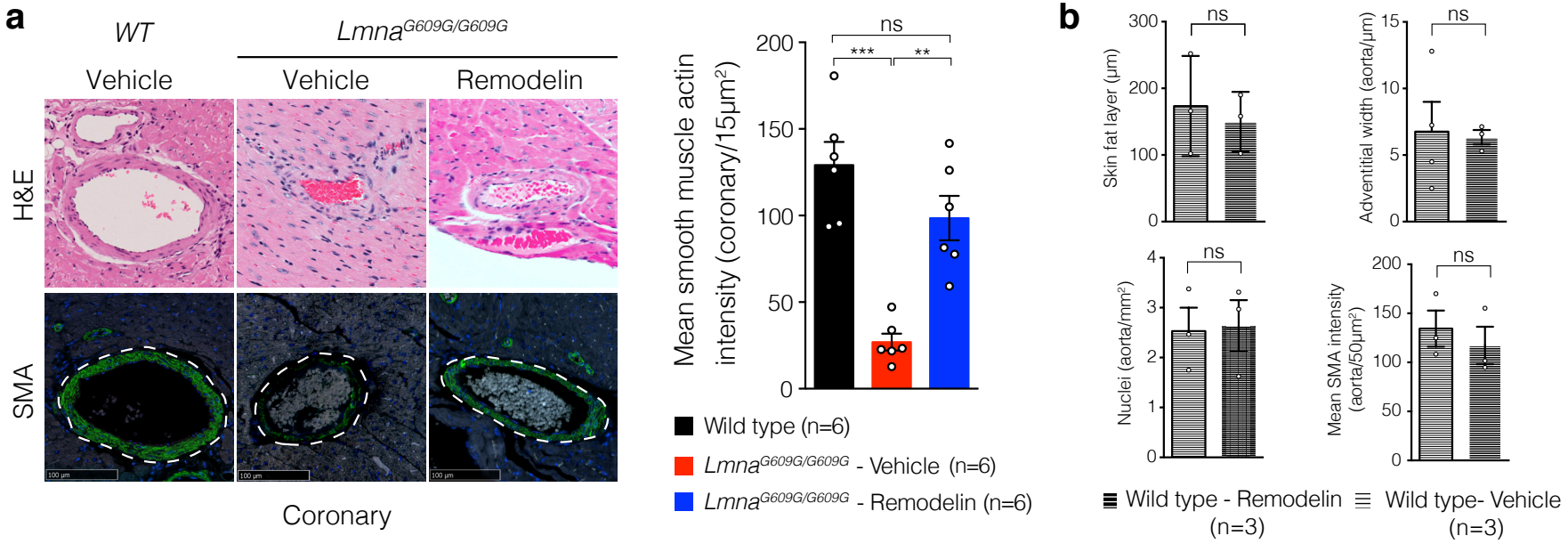
a
WT
Lmna G609G/G609G
Vehicle
Vehicle
Remodelin
H&E
SMA
Coronary
Mean smooth muscle actin intensity (coronary/15µm²)
ns
***
**
Wild type (n=6)
Lmna G609G/G609G - Vehicle (n=6)
Lmna G609G/G609G - Remodelin (n=6)
b
Skin fat layer (µm)
Adventitial width (aorta/µm)
Nuclei (aorta/mm²)
Mean SMA intensity (aorta/50µm²)
Wild type - Remodelin (n=3)
Wild type- Vehicle (n=3)

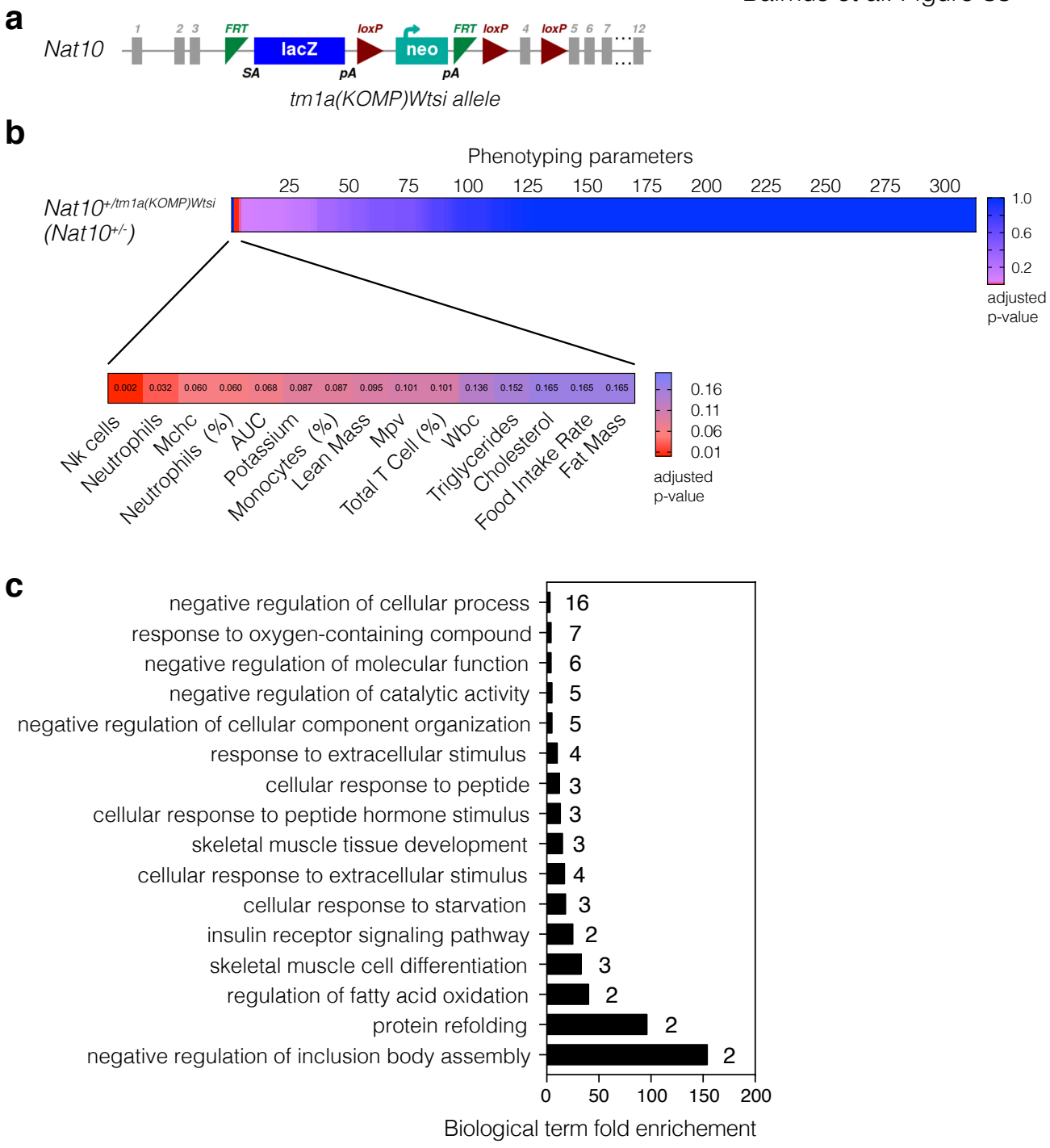
a
Nat10
1
2 3
FRT
lacZ
SA
loxP
pA
neo
FRT
pA
loxP
4
loxP
5 6 7 ... 12
tm1a(KOMP)Wtsi allele
b
Phenotyping parameters
25 50 75 100 125 150 175 200 225 250 275 300
Nat10+/tm1a(KOMP)Wtsi
(Nat10+/-)
1.0
0.6
0.2
adjusted
p-value
0.002 0.032 0.060 0.060 0.068 0.087 0.087 0.095 0.101 0.101 0.136 0.152 0.165 0.165 0.165
Nk cells
Neutrophils
Mchc
Neutrophils (%)
AUC
Potassium
Monocytes (%)
Lean Mass
Mpv
Total T Cell (%)
Wbc
Triglycerides
Cholesterol
Food Intake Rate
Fat Mass
0.16
0.11
0.06
0.01
adjusted
p-value
c
negative regulation of cellular process 16
response to oxygen-containing compound 7
negative regulation of molecular function 6
negative regulation of catalytic activity 5
negative regulation of cellular component organization 5
response to extracellular stimulus 4
cellular response to peptide 3
cellular response to peptide hormone stimulus 3
skeletal muscle tissue development 3
cellular response to extracellular stimulus 4
cellular response to starvation 3
insulin receptor signaling pathway 2
skeletal muscle cell differentiation 3
regulation of fatty acid oxidation 2
protein refolding 2
negative regulation of inclusion body assembly 2
0 50 100 150 200
Biological term fold enrichement

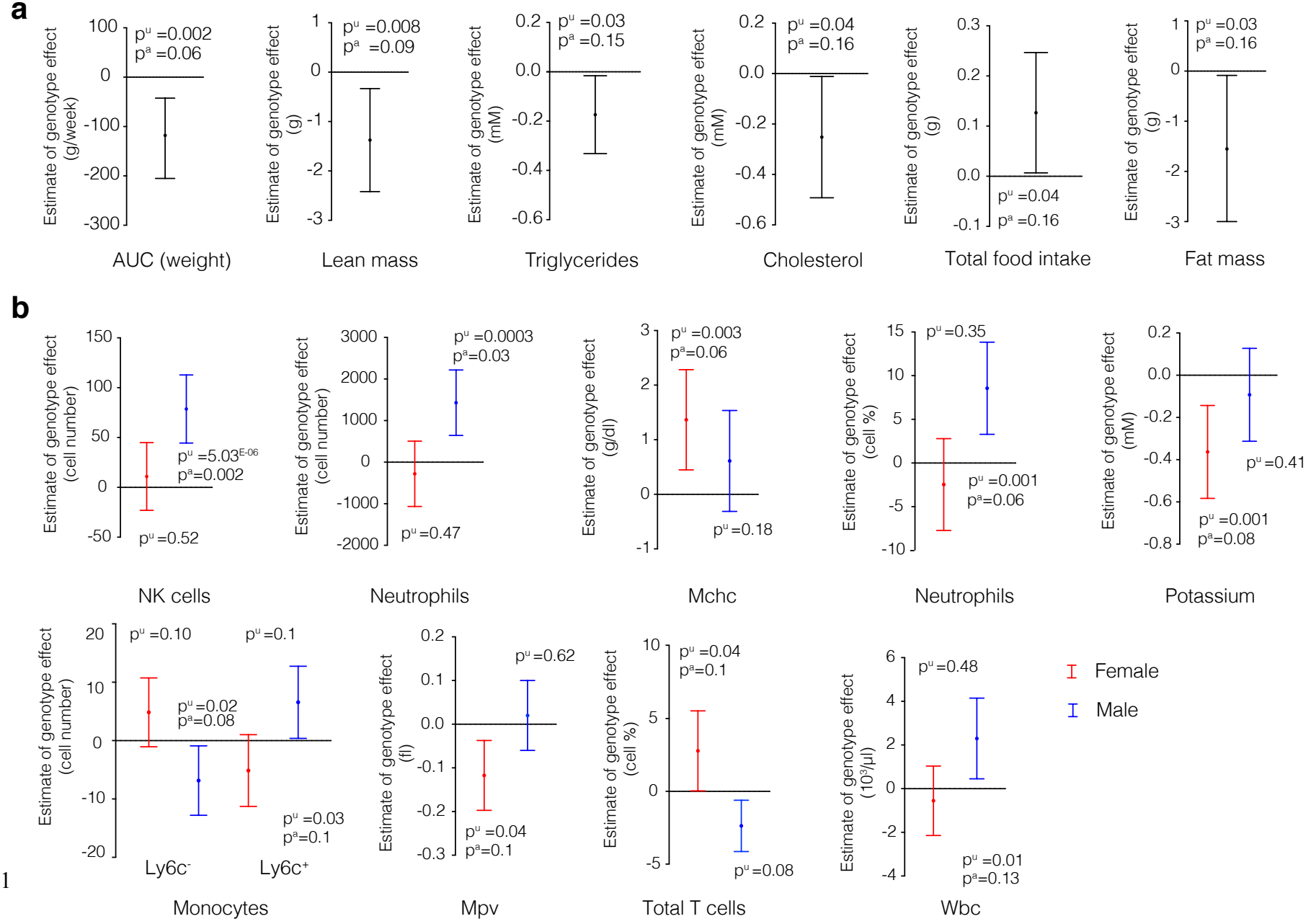
a
Estimate of genotype effect (g/week)
pu =0.002
pa =0.06
AUC (weight)
Estimate of genotype effect (g)
pu =0.008
pa =0.09
Lean mass
Estimate of genotype effect (mM)
pu =0.03
pa =0.15
Triglycerides
Estimate of genotype effect (mM)
pu =0.04
pa =0.16
Cholesterol
Estimate of genotype effect (g)
pu =0.04
pa =0.16
Total food intake
Estimate of genotype effect (g)
pu =0.03
pa =0.16
Fat mass
b
Estimate of genotype effect (cell number)
pu =5.03E-06
pa=0.002
pu =0.52
NK cells
Estimate of genotype effect (cell number)
pu =0.0003
pa=0.03
pu =0.47
Neutrophils
Estimate of genotype effect (g/dl)
pu =0.003
pa=0.06
pu =0.18
Mchc
Estimate of genotype effect (cell %)
pu =0.35
pu =0.001
pa=0.06
Neutrophils
Estimate of genotype effect (mM)
pu =0.41
pu =0.001
pa=0.08
Potassium
Estimate of genotype effect (cell number)
pu =0.10
pu =0.1
pu =0.02
pa=0.08
pu =0.03
pa=0.1
Ly6c-
Ly6c+
Monocytes
Estimate of genotype effect (fl)
pu =0.62
pu =0.04
pa=0.1
Mpv
Estimate of genotype effect (cell %)
pu =0.04
pa=0.1
pu =0.08
Total T cells
Estimate of genotype effect (10³/µl)
pu =0.48
pu =0.01
pa=0.13
Wbc
Female
Male

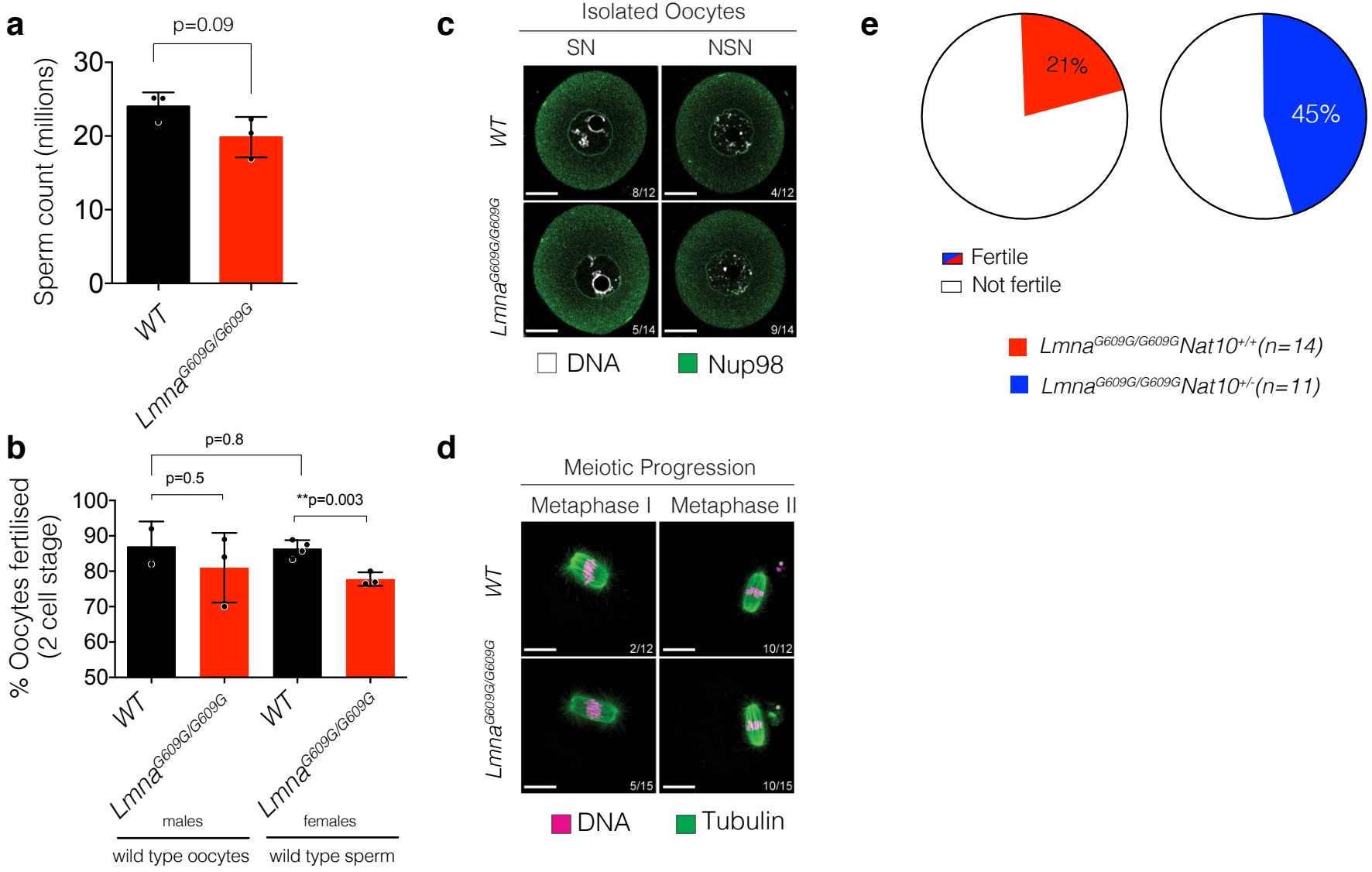
a
p=0.09
Sperm count (millions)
30
20
10
0
WT
LmnaG609G/G609G
b
p=0.8
p=0.5
**p=0.003
% Oocytes fertilised (2 cell stage)
100
90
80
70
60
50
WT
LmnaG609G/G609G
WT
LmnaG609G/G609G
males
females
wild type oocytes
wild type sperm
c
Isolated Oocytes
SN
NSN
WT
LmnaG609G/G609G
8/12
4/12
5/14
9/14
DNA
Nup98
d
Meiotic Progression
Metaphase I
Metaphase II
WT
LmnaG609G/G609G
2/12
10/12
5/15
10/15
DNA
Tubulin
e
21%
45%
Fertile
Not fertile
LmnaG609G/G609GNat10+/+(n=14)
LmnaG609G/G609GNat10+/-(n=11)

2

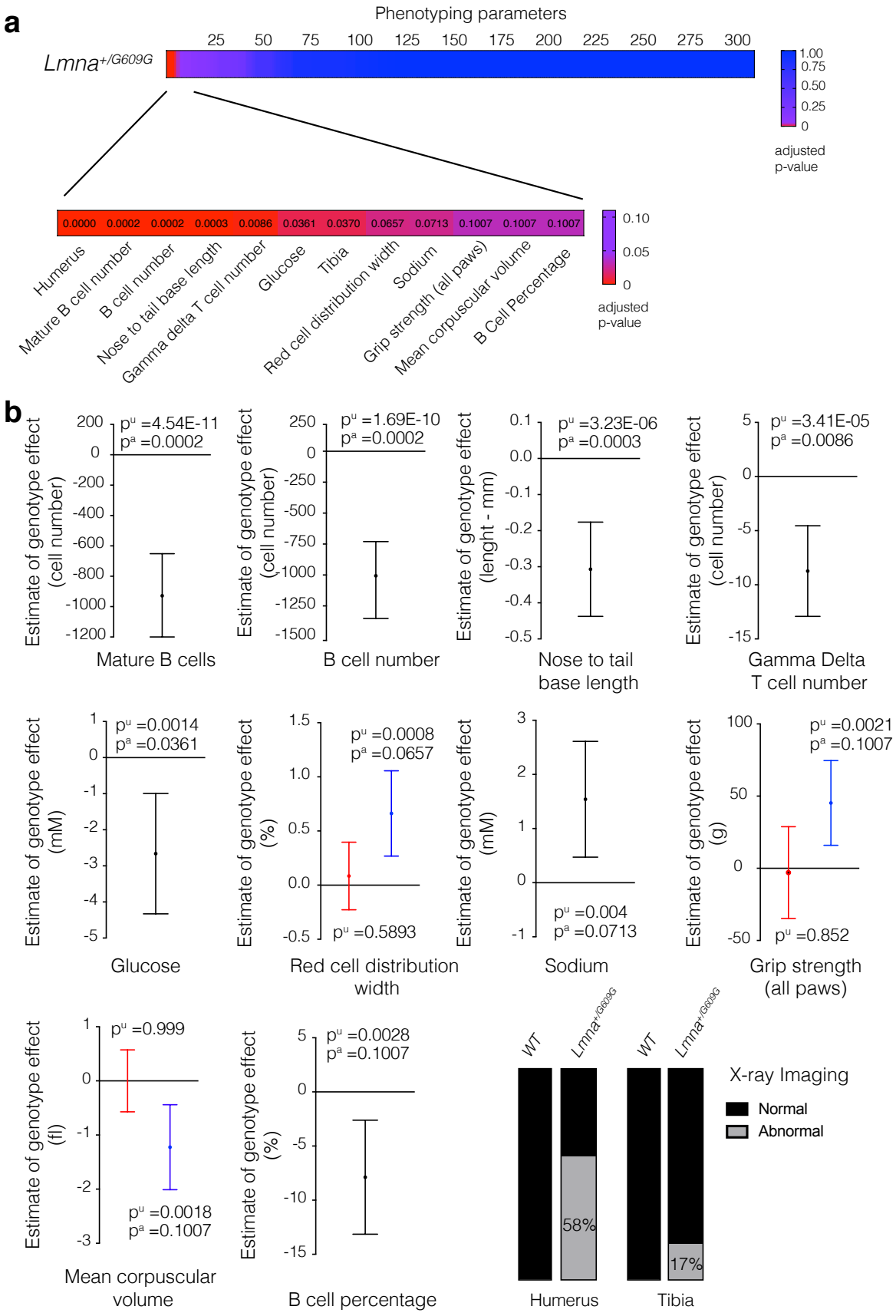
a
Phenotyping parameters
25 50 75 100 125 150 175 200 225 250 275 300
Lmna+/G609G
1.00
0.75
0.50
0.25
0
adjusted p-value
0.0000 0.0002 0.0002 0.0003 0.0086 0.0361 0.0370 0.0657 0.0713 0.1007 0.1007 0.1007
0.10
0.05
0
adjusted p-value
Humerus
Mature B cell number
B cell number
Nose to tail base length
Gamma delta T cell number
Glucose
Tibia
Red cell distribution width
Sodium
Grip strength (all paws)
Mean corpuscular volume
B Cell Percentage
b
Estimate of genotype effect (cell number)
pu =4.54E-11
pa =0.0002
Mature B cells
Estimate of genotype effect (cell number)
pu =1.69E-10
pa =0.0002
B cell number
Estimate of genotype effect (lenght - mm)
pu =3.23E-06
pa =0.0003
Nose to tail base length
Estimate of genotype effect (cell number)
pu =3.41E-05
pa =0.0086
Gamma Delta T cell number
Estimate of genotype effect (mM)
pu =0.0014
pa =0.0361
Glucose
Estimate of genotype effect (%)
pu =0.0008
pa =0.0657
pu =0.5893
Red cell distribution width
Estimate of genotype effect (mM)
pu =0.004
pa =0.0713
Sodium
Estimate of genotype effect (g)
pu =0.0021
pa =0.1007
pu =0.852
Grip strength (all paws)
Estimate of genotype effect (fl)
pu =0.999
pu =0.0018
pa =0.1007
Mean corpuscular volume
Estimate of genotype effect (%)
pu =0.0028
pa =0.1007
B cell percentage
WT
Lmna+/G609G
WT
Lmna+/G609G
X-ray Imaging
Normal
Abnormal
58%
17%
Humerus
Tibia

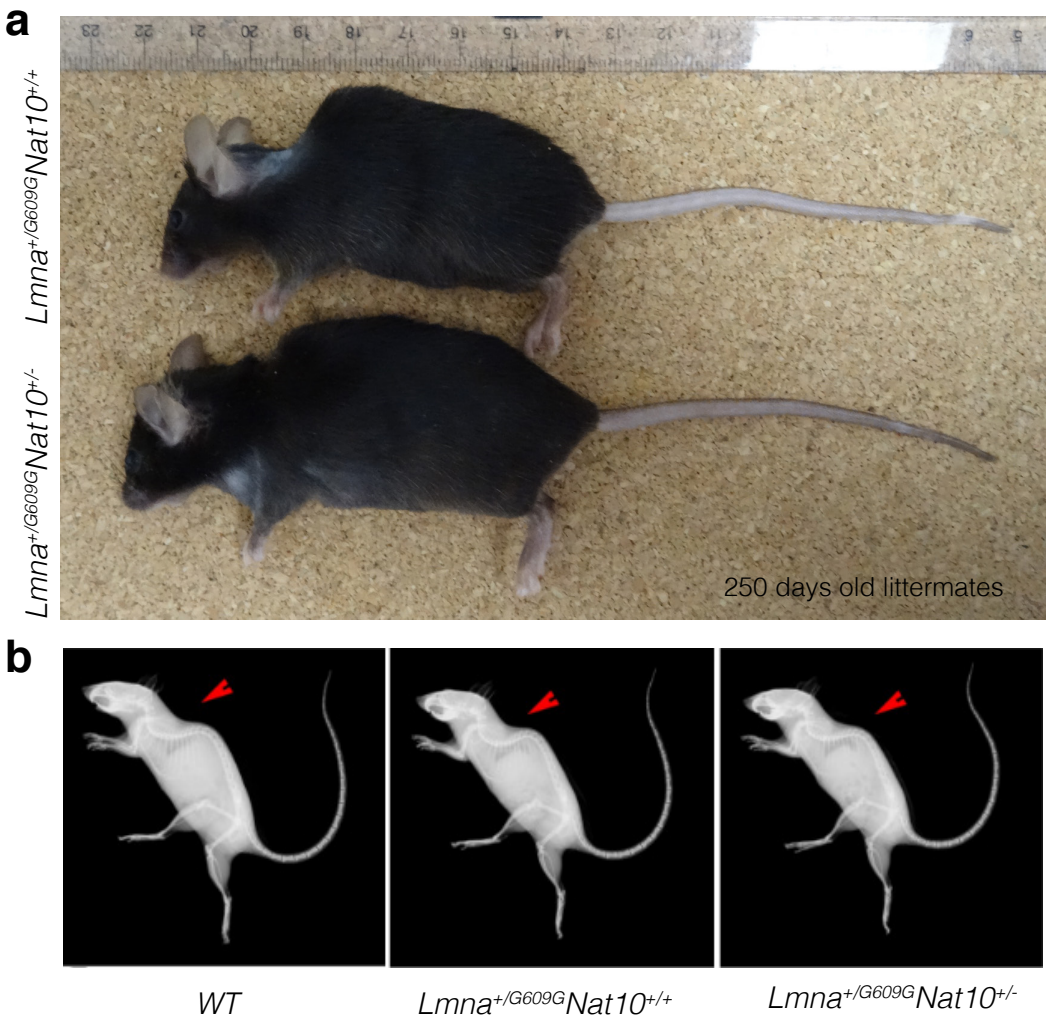
a
Lmna+/G609GNat10+/+
Lmna+/G609GNat10+/-
250 days old littermates
b
WT
Lmna+/G609GNat10+/+
Lmna+/G609GNat10+/-

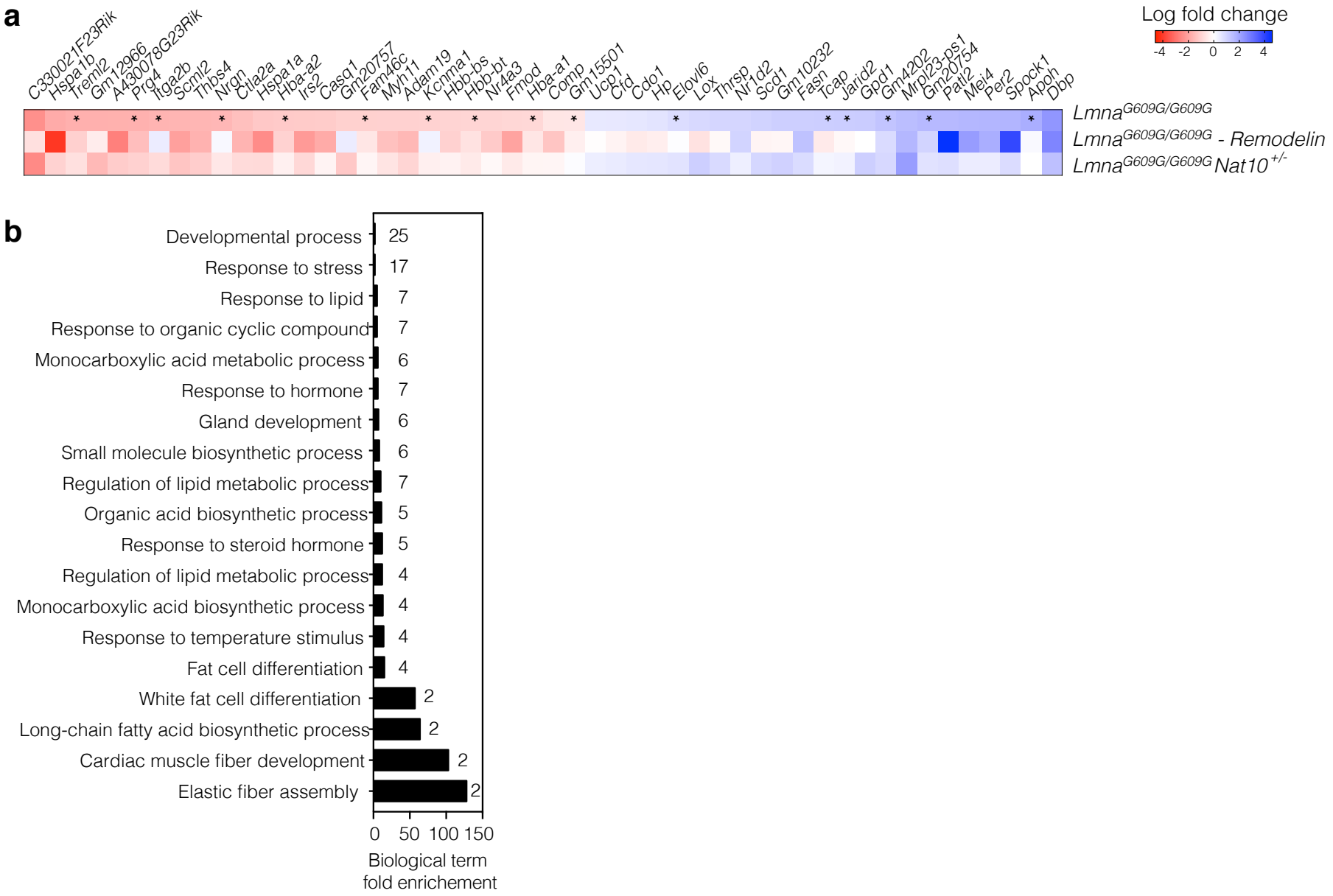
a
Log fold change
-4 -2 0 2 4
C330021F23Rik
Hspa1b
Treml2
Gm12966
A430078G23Rik
Prg4
Itga2b
Scml2
Thbs4
Nrgn
Ctla2a
Hspa1a
Hba-a2
Irs2
Casq1
Gm20757
Fam46c
Myh11
Adam19
Kcnma1
Hbb-bs
Hbb-bt
Nr4a3
Fmod
Hba-a1
Comp
Gm15501
Ucp1
Cfd
Cdo1
Hp
Elovl6
Lox
Thrsp
Nr1d2
Scd1
Gm10232
Fasn
Tcap
Jarid2
Gpd1
Gm4202
Mrpl23-ps1
Gm20754
Patl2
Mei4
Per2
Spock1
Apoh
Dbp
Lmna G609G/G609G
Lmna G609G/G609G - Remodelin
Lmna G609G/G609G Nat10 +/-
b
Developmental process 25
Response to stress 17
Response to lipid 7
Response to organic cyclic compound 7
Monocarboxylic acid metabolic process 6
Response to hormone 7
Gland development 6
Small molecule biosynthetic process 6
Regulation of lipid metabolic process 7
Organic acid biosynthetic process 5
Response to steroid hormone 5
Regulation of lipid metabolic process 4
Monocarboxylic acid biosynthetic process 4
Response to temperature stimulus 4
Fat cell differentiation 4
White fat cell differentiation 2
Long-chain fatty acid biosynthetic process 2
Cardiac muscle fiber development 2
Elastic fiber assembly 2
0 50 100 150
Biological term
fold enrichement

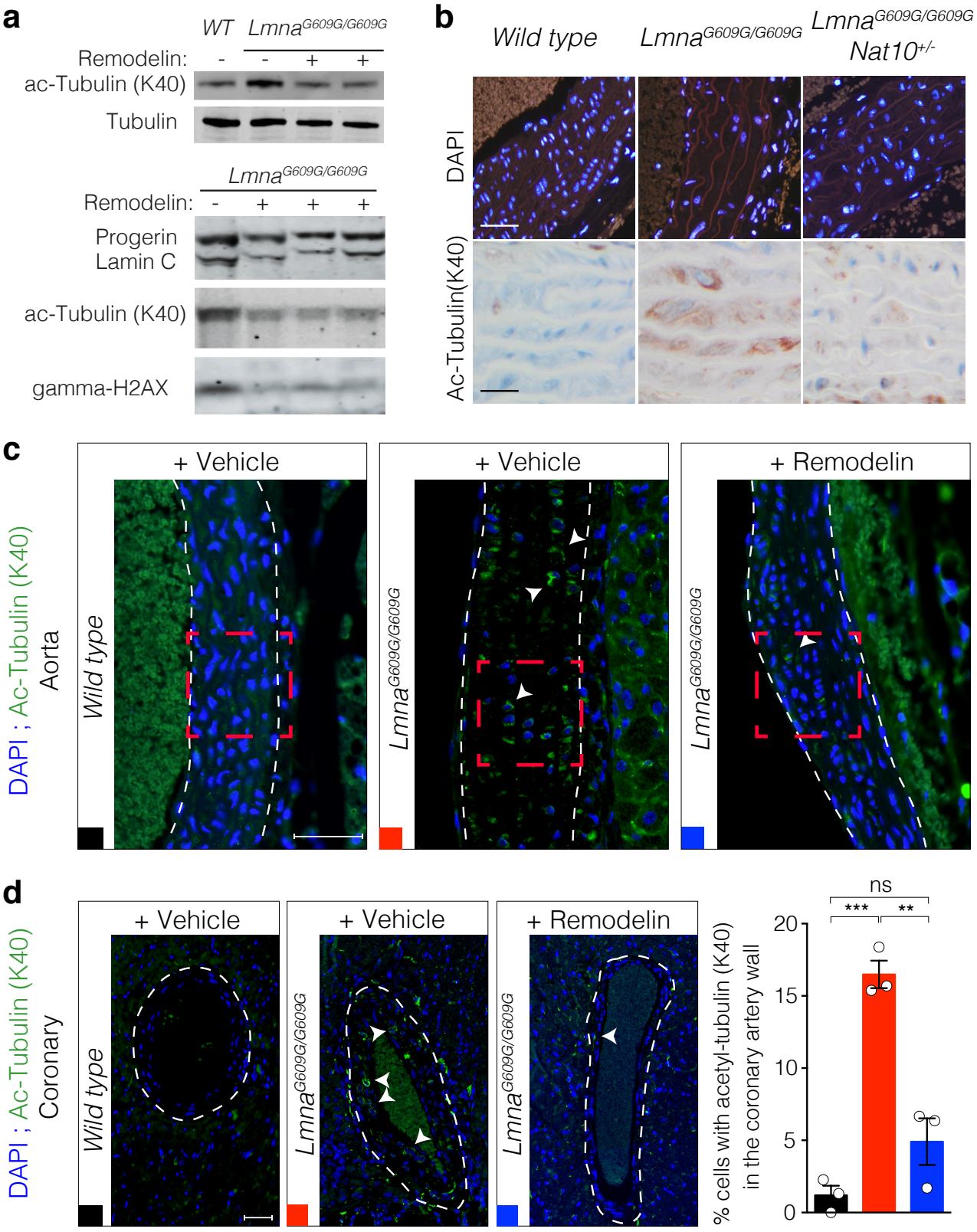
a
WT
Lmna G609G/G609G
Remodelin:
ac-Tubulin (K40)
Tubulin
Lmna G609G/G609G
Remodelin:
Progerin
Lamin C
ac-Tubulin (K40)
gamma-H2AX
b
Wild type
Lmna G609G/G609G
Lmna G609G/G609G Nat10 +/-
DAPI
Ac-Tubulin(K40)
c
DAPI ; Ac-Tubulin (K40)
Aorta
+ Vehicle
+ Vehicle
+ Remodelin
Wild type
Lmna G609G/G609G
Lmna G609G/G609G
d
DAPI ; Ac-Tubulin (K40)
Coronary
+ Vehicle
+ Vehicle
+ Remodelin
Wild type
Lmna G609G/G609G
Lmna G609G/G609G
% cells with acetyl-tubulin (K40) in the coronary artery wall
ns
***
**
20
15
10
5
0

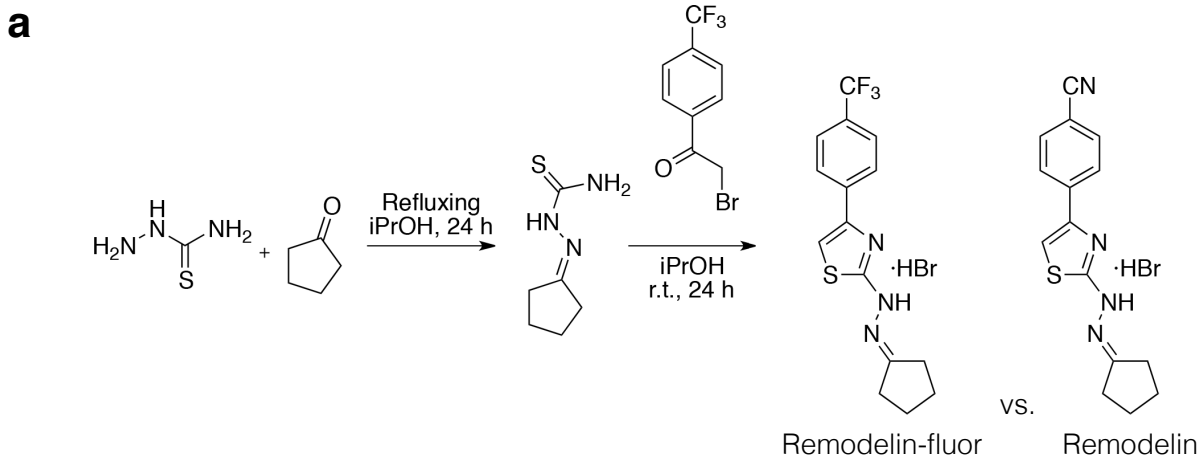
a
Refluxing
iPrOH, 24 h
iPrOH
r.t., 24 h
·HBr
Remodelin-fluor
vs.
Remodelin

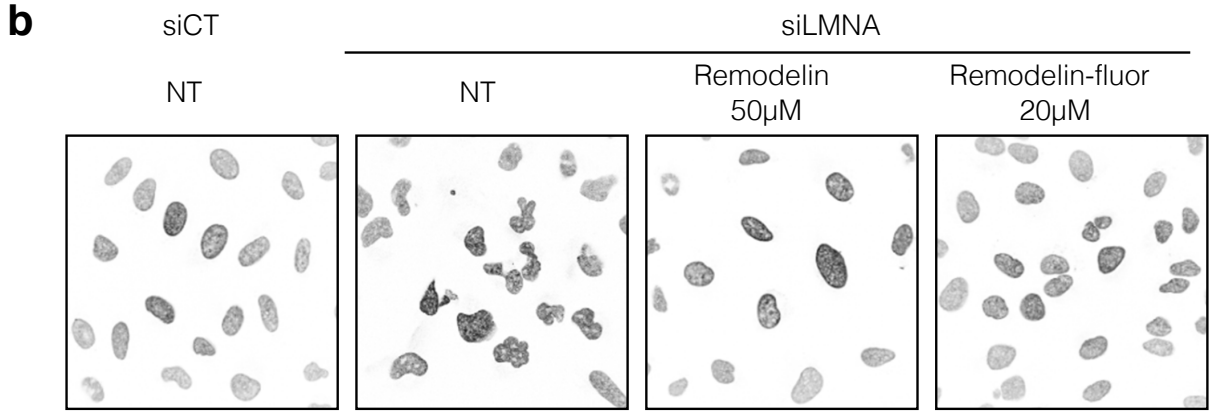
b
siCT
siLMNA
NT
NT
Remodelin
50μM
Remodelin-fluor
20μM

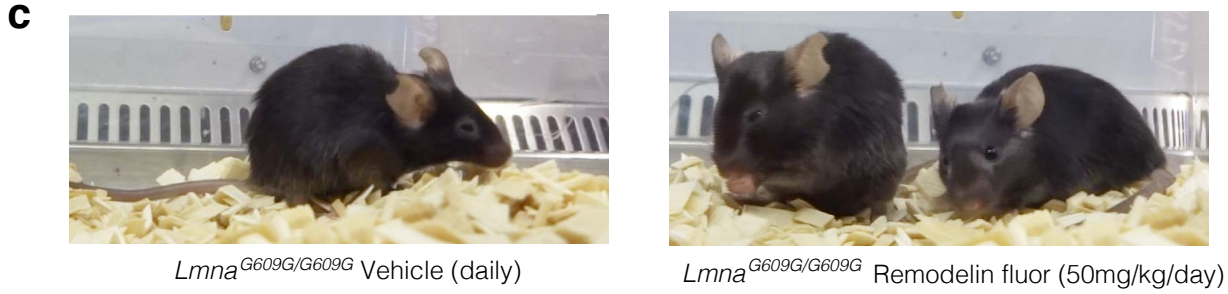
c
Lmna G609G/G609G Vehicle (daily)
Lmna G609G/G609G Remodelin fluor (50mg/kg/day)

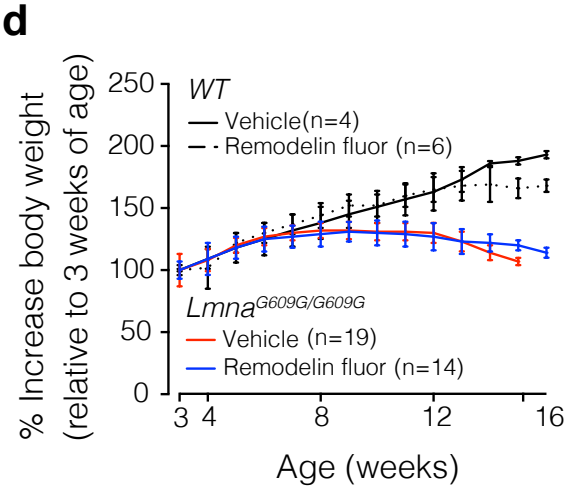
d
% Increase body weight
(relative to 3 weeks of age)
WT
Vehicle(n=4)
Remodelin fluor (n=6)
Lmna G609G/G609G
Vehicle (n=19)
Remodelin fluor (n=14)
Age (weeks)

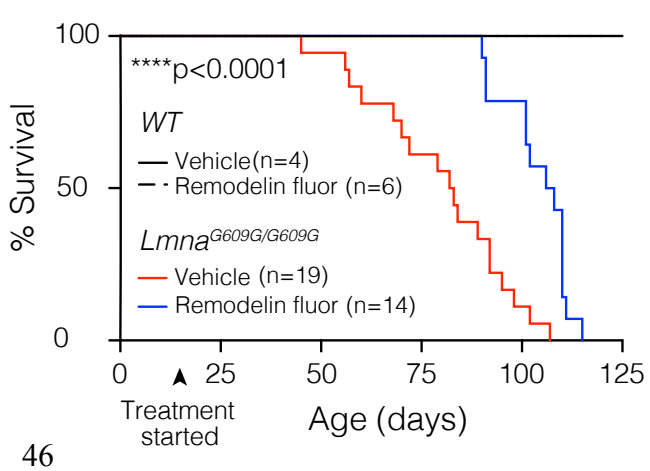
e
% Survival
****p<0.0001
WT
Vehicle(n=4)
Remodelin fluor (n=6)
Lmna G609G/G609G
Vehicle (n=19)
Remodelin fluor (n=14)
Treatment
started
Age (days)